

RESEARCH ARTICLE

Geometric latches enable tuning of ultrafast, spring-propelled movements

Sarah J. Longo^{1,*,\ddagger}, Ryan St. Pierre^{2,\ddagger}, Sarah Bergbreiter³, Suzanne Cox¹, Benjamin Schelling¹ and S. N. Patek^{1,\S}

ABSTRACT

The smallest, fastest, repeated-use movements are propelled by power-dense elastic mechanisms, yet the key to their energetic control may be found in the latch-like mechanisms that mediate transformation from elastic potential energy to kinetic energy. Here, we tested how geometric latches enable consistent or variable outputs in ultrafast, spring-propelled systems. We constructed a reduced-order mathematical model of a spring-propelled system that uses a torque reversal (over-center) geometric latch. The model was parameterized to match the scales and mechanisms of ultrafast systems, specifically snapping shrimp. We simulated geometric and energetic configurations that enabled or reduced variation of strike durations and dactyl rotations given variation of stored elastic energy and latch mediation. Then, we collected an experimental dataset of the energy storage mechanism and ultrafast snaps of live snapping shrimp (*Alpheus heterochaelis*) and compared our simulations with their configuration. We discovered that snapping shrimp deform the propodus exoskeleton prior to the strike, which may contribute to elastic energy storage. Regardless of the amount of variation in spring loading duration, strike durations were far less variable than spring loading durations. When we simulated this species' morphological configuration in our mathematical model, we found that the low variability of strike duration is consistent with their torque reversal geometry. Even so, our simulations indicate that torque reversal systems can achieve either variable or invariant outputs through small adjustments to geometry. Our combined experiments and mathematical simulations reveal the capacity of geometric latches to enable, reduce or enhance variation of ultrafast movements in biological and synthetic systems.

KEY WORDS: Elastic mechanism, *Alpheus heterochaelis*, Latch-mediated spring actuation, Torque reversal, Snapping shrimp

INTRODUCTION

Many organisms and engineered devices use systems of latches and springs to perform extremely rapid motions, including the impressive jumps of fleas and locusts (Bennet-Clark and Lucey, 1967; Bennet-Clark, 1975), shell-smashing strikes of mantis shrimp (Patek et al., 2007; Patek, 2019; Steinhardt et al., 2021) and many

robotic jumpers (Armour et al., 2007; Aguilar et al., 2012; Ribak, 2020; Zhang et al., 2020). These systems use a class of mechanisms termed latch-mediated spring actuation (LaMSA) (Longo et al., 2019). LaMSA systems store energy and actuate movement with springs mediated by latch mechanisms (Gronenberg, 1996; Patek et al., 2011; Sakes et al., 2016; Ilton et al., 2018; Longo et al., 2019). LaMSA can yield high mass-specific power outputs and remarkable accelerations. Assuming switch-like (on–off) latches, tuning of LaMSA outputs should only occur during spring loading (Galantis and Woledge, 2003; Kagaya and Patek, 2016; Roberts, 2019). However, recently modeled and biological LaMSA systems with realistic, non-idealized dynamics can adjust their movement using latch mediation (Ilton et al., 2018; Reynaga et al., 2019; Divi et al., 2020). These discoveries encourage new emphasis on the ability to vary (i.e. tunability) of ultrafast systems – especially through latch mechanisms – for a variety of potential performance benefits (Ilton et al., 2018; Abbott et al., 2019; Bolmin et al., 2019; Divi et al., 2020; Bolmin et al., 2021; Steinhardt et al., 2021).

Latches separate and energetically mediate spring loading and spring propulsion in LaMSA systems. Latches and their associated dynamics modify forces, moment arms, geometric configurations and other internal system parameters to mediate the timing or magnitude of energy flow. Perhaps owing to the historical assumption of instantaneous latch dynamics (i.e. latches as on–off switches), coupled with the challenges of imaging these extremely fast, small and brief movements in living organisms, only recently have latch dynamics been analyzed in depth (Hyun et al., 2023; Ilton et al., 2018; Bolmin et al., 2019; 2021; Steinhardt et al., 2021). For example, an integrative engineering and biomechanics analysis of contact latches (latches operating through frictional, contact-based interactions of two structures) based on Dracula snap-jaw ants (*Mystrium camillae*) revealed that latch shape and removal speed mediate both the timing and magnitude of energy flow to influence output performance (Divi et al., 2020). Latches are central to mediating the flow of energy through these systems, especially for achieving cascading mechanical power amplification alongside repeated use (Ilton et al., 2018; Longo et al., 2019; Patek, 2019; Divi et al., 2020; Steinhardt et al., 2021; Hyun et al., 2023). Here, we tested the role of latch dynamics in reducing or enabling kinematic variation in LaMSA systems, specifically in terms of the role of geometry in the dynamics of the torque reversal latches found in snapping shrimp.


Torque reversal latches (also termed over-center latches) in LaMSA systems are a type of geometric latch in which the sign of the torque reverses when a rotating system transitions from spring loaded and latched to unlatched and spring propelled (Fig. 1) (Bennet-Clark and Lucey, 1967; Heitler, 1974; Gorb, 2004; Burrows, 2009; Koh et al., 2015; Kaji et al., 2018; Longo et al., 2018; Patek and Longo, 2018; Longo et al., 2019; Kallal et al., 2021; Steinhardt et al., 2021). Torque reversal latches can thus directly mediate the transformation of elastic potential energy to

¹Department of Biology, Duke University, Durham, NC 27708, USA. ²Department of Mechanical and Aerospace Engineering, University at Buffalo, Buffalo, NY 14260, USA. ³Department of Mechanical Engineering, Carnegie Mellon University, Pittsburgh, PA 15213, USA.

*Present address: Department of Biological Sciences, Towson University, Towson, MD 21252, USA.

^{\ddagger}These authors contributed equally to this work

^{\S}Author for correspondence (snp2@duke.edu)

 S.J.L., 0000-0001-5429-2473; R.S., 0000-0003-4609-5642; S.B., 0000-0003-2735-0206; S.C., 0000-0002-9704-0716; S.N.P., 0000-0001-9738-882X

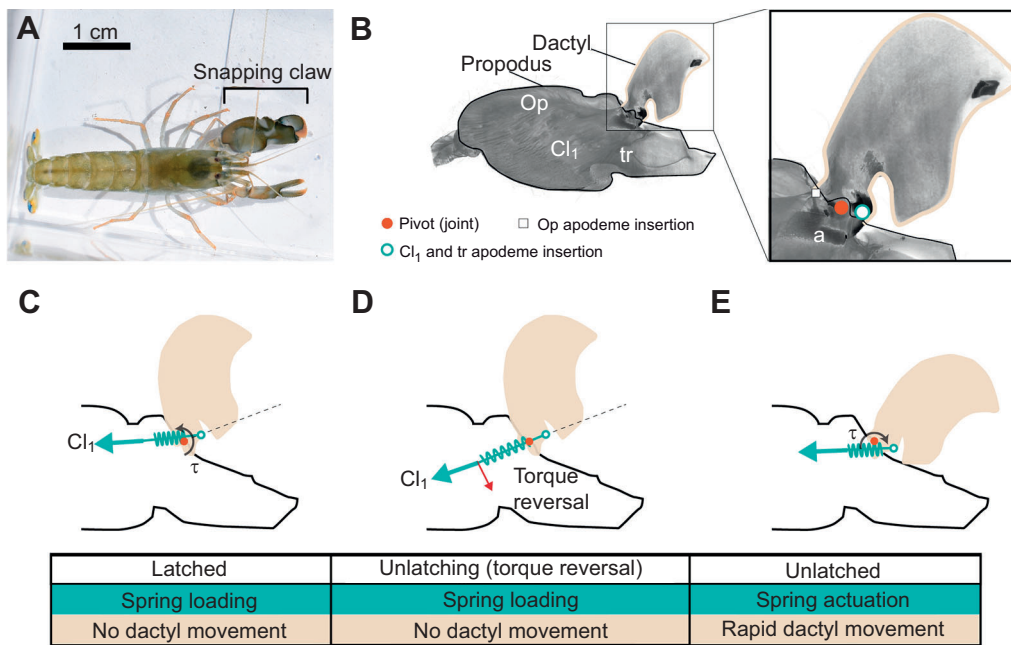


Fig. 1. A torque reversal latch mediates the transition from elastic energy storage to rapid dactyl closure in snapping shrimp. (A) *Alpheus heterochaelis* has two claws; one is exceptionally large (left claw, in this image). Snapping shrimp use the large claw to snap rapidly and generate a water jet and cavitation. Dorsal view with anterior to the right. (B) The large claw's dactyl rotates rapidly around a pivot (orange circle) through the action of the opener (Op), closer (Cl₁) and trigger (tr, or Cl₂ muscles; Ritzmann, 1974). These images are dye-enhanced micro-CT reconstructions of a dactyl that is not fully open and is unlatched. The magnified inset highlights the positions of the apodeme insertions (white square and turquoise circle) around the pivot (orange circle). In this dactyl configuration, the opener muscle attachment is positioned proximally (white square) to the pivot (orange circle). Cl₁ and tr apodeme (a) attachments (turquoise circle) are positioned distally to the pivot. In this and subsequent images, distal is to the right. (C) This schematic depicts the hypothesized torque-reversal latch in *A. heterochaelis* as originally described by Ritzmann (1974). When the dactyl is in the latched position, the closer apodeme insertion (turquoise circle) is positioned distally to the pivot formed by the joint between the dactyl and propodus (orange circle). In this orientation, force from contraction of the closer muscle (Cl₁) does not generate a net closing torque (τ) on the dactyl. Instead, elastic energy is stored via an elastic mechanism (stretched turquoise spring). (D) Subsequent activation of the trigger muscle then shifts the position of the closer apodeme insertion such that the system starts to unlatch as the net torque on the dactyl suddenly reverses sign. (E) Immediately after torque reversal, elastic potential energy is rapidly transformed into kinetic energy to power the extremely rapid dactyl snap.

kinetic energy in LaMSA systems (Steinhardt et al., 2021). Torque reversal also serves as a mechanism enabling organisms to switch between muscle-driven and spring-driven movement (Burrows and Morris, 2003; Steinhardt et al., 2021). Here, we focused on a torque reversal mechanism found in some snapping shrimp species in the genus *Alpheus* (Fig. 1) (Ritzmann, 1974; Kaji et al., 2018; Chow et al., 2021). The torque reversal latching mechanism of *Alpheus heterochaelis* is hypothesized to operate as follows: (1) when the dactyl (i.e. the final segment of the appendage) is fully open, the geometry is such that a dactyl closer muscle loads energy into elastic elements rather than closing the dactyl, and (2) unlatching occurs when a trigger muscle shifts the geometry, suddenly reversing the sign of torque (Ritzmann, 1974).

Multiple parameters of a LaMSA torque reversal mechanism are central to understanding and testing the potential for enhancing or reducing variation in the kinematics of spring-propelled systems (Table 1). Considering Fig. 1 and its representation of the snapping shrimp mechanism, if the relative position of the spring attachment point to the pivot point results in an increasing torque on the dactyl about the pivot point in the opening direction, then elastic elements are loaded by the closer muscle. Otherwise, the dactyl rotates closed by simply contracting the closer muscle (muscle-driven actuation). When the dactyl is oriented such that the elastic mechanism is loaded, peak torque in the opening direction occurs when loading is complete. After the loading process, the unlatching process begins. During unlatching, the line of action of the force from the loaded

spring is rotated toward the pivot point, which causes the torque on the dactyl about the pivot point to decrease until reaching zero. Additional energy need not be loaded into the spring during this unlatching process. When the line of actuation of the force is directly through the pivot point, the torque is equal to zero and the dactyl is unlatched. As soon as the spring is rotated past this zero-point, the torque reverses sign, and the spring applies torque to the dactyl, causing it to close as the spring recoils. Because the line of action of the spring force continues to rotate along with the rotating dactyl, the magnitude of torque continues to increase and accelerate the dactyl, resulting in rapid closure. In each of these dynamic states, small adjustments to the geometry, dynamics or energetics of the system have the potential to reduce or enhance variation of the output movement relative to the variation in stored elastic energy – extending to configurations in which torque reversal latching no longer occurs.

Although the above description of LaMSA torque reversal captures the geometric basis for the transition from a latched to an unlatched state, potentially tunable features of the dynamic process of transforming loaded elastic energy into kinetic energy may also affect the potential for enhancing or reducing variation in the kinematics of spring-propelled systems. Dactyl closing kinematics could be varied by adjusting the energy loaded into the system, such as by varying energy loading duration and rate. In this simplest case, a system would exhibit a positive correlation between elastic potential energy and kinetic energy, because kinetic energy is equal to elastic potential energy minus losses from friction and drag.

Table 1. Modeled and measured parameters

Symbol	Description	Base units	Comments
Physical parameters			
D	Diameter of dactyl	m	Estimated as a cylinder
L	Length of dactyl	m	Estimated as a cylinder
m	Mass of dactyl	kg	Estimated as the volume of a cylinder multiplied by the density of water
I	Mass moment of inertia of the dactyl at the pivot point	kg m ²	Calculated for a cylinder using the parallel axis theorem
a_h	Horizontal distance of the apodeme insertion point	m	Measured from biological data, and measured along the horizontal of the cylinder in the model (Fig. 2A)
a_v	Vertical distance of the apodeme insertion point	m	Measured from biological data, and measured along the vertical of the cylinder in the model (Fig. 2A)
k_t	Spring constant of apodeme	N m ⁻¹	Estimated from literature
Mathematical model parameters			
τ	Torque on dactyl	N m	Calculated from spring deformation, relative positioning of spring placement and pivot point, and dactyl rotation
θ	Dactyl angle	deg	Measured clockwise from the y-axis in the model (Fig. 2A)
θ_{ul}	Unlatching angle	deg	Measured counterclockwise from the negative x-axis in the model (Fig. 2A)
No symbol	Energy in system	J	Calculated as the product of energy loading duration and energy loading rate, appears in Eqn 1 as $\Delta t(\Delta E/\Delta t)$
Δt	Energy loading duration	s	Used to parameterize the energy inputs into the model (Fig. 3A)
$\Delta E/\Delta t$	Energy loading rate	J s ⁻¹	Used to parameterize the energy inputs into the model (Fig. 3A)
$d\theta_{ul}/dt$	Unlatching rate	deg s ⁻¹	Used to parameterize the unlatching of the model (Fig. 3A)
Latch parameters			
θ_{tr}	Torque reversal angle	deg	Calculated as the arctangent of a_v/a_h (Fig. 2C)
$\theta(0)$	Dactyl starting angle	deg	Initial angle of θ at time $t=0$ (Fig. 2B)

Variation in kinematics can also be achieved through geometric adjustments that change the unlatching rate. The unlatching rate mediates the exchange of energy from stored elastic energy to kinetic energy. How torque evolves after torque reversal also directly affects how kinematics can be varied through the geometric and dynamic properties of the torque reversal mechanism as described above. It should be noted that many snapping shrimp also have an adhesive disk, which plays a role in latching; in *A. heterochaelis*, the focus of the present study, the adhesive latch is small and thought to play a minimal role in latching/unlatching (Ritzmann, 1974).

Snapping shrimp perform remarkable feats with their ultrafast LaMSA mechanism. Their rapid strikes – completed in less than 1 ms – generate such a fast water jet that cavitation forms behind it, resulting in a shooting cavitation bubble that can move at over 30 m s⁻¹ (Versluis et al., 2000; Lohse et al., 2001). Their snaps are used for a number of ecologically important functions, including communication, territorial defense, intraspecific and interspecific agonistic interactions, prey capture and even tunnelling (Winn and Hazlett, 1962; Schein, 1977; Knowlton and Keller, 1982; Beal, 1983; Vermeij, 1987; Hughes, 1996a,b; Schmitz and Herberholz, 1998; Herberholz and Schmitz, 1999; Silliman et al., 2003; Dinh et al., 2020; Dinh and Radford, 2021; Dinh, 2022; Dinh and Patek, 2022; Kingston et al., 2022). Snapping shrimp claws have been examined in the contexts of their material properties and ability to consistently and efficiently generate cavitation and plasma (Koukouviniis et al., 2017; Alam et al., 2018; Amini et al., 2018; Tang and Staack, 2019). Even with sustained attention on these remarkable animals, it remains uncertain how they store elastic energy and whether torque reversal latching is used for enhancing or reducing the variation of their strikes amidst the diverse behavioral and ecological contexts for their snaps. For instance, an increased scope for strike variation could allow snapping shrimp (or any biomechanical system) to adjust output in response to different stimuli, such as prey type. In contrast, mechanisms that reduce strike

variation in response to environmental fluctuations or short-term perturbations could also be favorable.

We addressed the following questions in this study: (1) How do snapping shrimp store elastic energy and when is elastic energy stored and released relative to the timing of cocking and release of the dactyl? (2) At the scale and configuration of snapping shrimp, what are the dynamic consequences of geometric parameter combinations (in terms of dactyl starting angle and torque reversal angle) for the presence and absence of latching by torque reversal and for the enhancement or reduction of variable kinematics given varying elastic potential energy storage? (3) Based on a large experimental dataset that encompasses individual variation in snapping behavior, which realm of torque reversal dynamics modeling in question 2 is used by *A. heterochaelis* snapping shrimp such that their torque reversal mechanism enhances or reduces variation of their strikes?

To address these questions, we developed a reduced-order model of a LaMSA torque reversal mechanism similar to the one found in snapping shrimp (Fig. 2, Table 1). Our goal was to simulate how variable and consistent outputs can be achieved through modifications to the torque reversal mechanism without exact predictions of performance. We probed the boundary between torque reversal configurations that can enable LaMSA or can only mediate direct muscle contractions without latch-like dynamics. We performed an experimental analysis of the relative variability of elastic energy storage and strike kinematics in live snapping shrimp. Although much of the historical focus on these systems has emphasized ultra-high speeds or accelerations, we focus here on the two parameters for these strikes: dactyl rotation and strike duration. This approach keeps the same units for loading, unlatching and striking, which is necessary for comparisons of variation between these phases of the mechanism. We tested whether snapping shrimp follow the predictions for enhancing or reducing the variation of their strikes relative to their variation in energy loading using simulations with their particular torque reversal configuration.

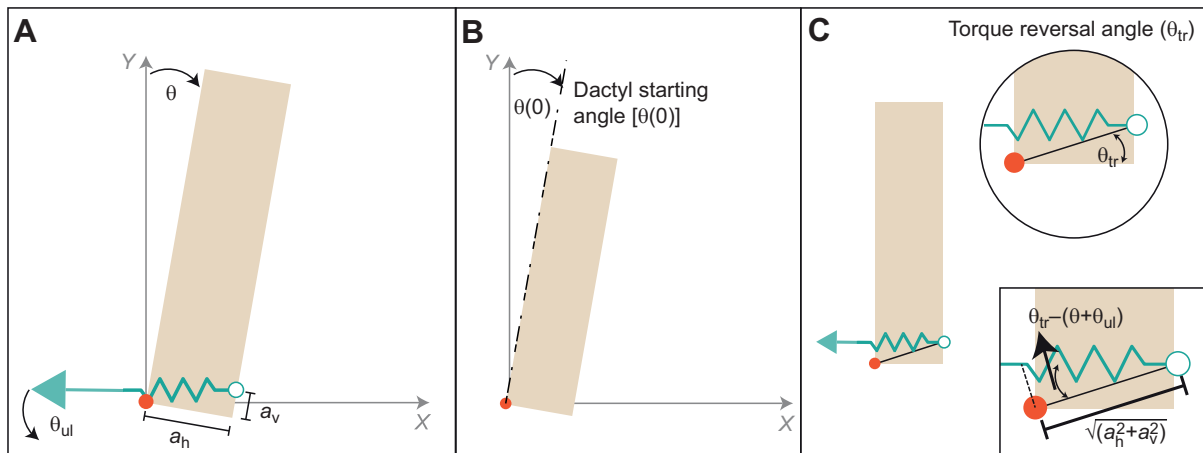


Fig. 2. We simulated a spring-actuated, torque reversal mechanism with similar scale and dynamics to the snap mechanism in snapping shrimp.

(A) This schematic of the template model shows the coordinate system oriented to mirror the biological system in Fig. 1: the dactyl (tan box; planar, lateral view of the modeled cylinder), the dactyl's angular rotation (θ), pivot (orange circle) spring attachment location (turquoise circle), spring (turquoise spring) and spring force (turquoise arrow). We simulated the absolute motion of the spring force through the unlatching angle (θ_{ul}) as it rotated through the torque reversal angle. The torque reversal angle was defined by the relative horizontal (a_h) and vertical (a_v) distances from the pivot point to the spring attachment point. (B) The starting angle of the dactyl was defined as an initial rotational position at time 0. (C) Torque reversal angle was defined as the arctangent of the relative horizontal (a_h) and vertical (a_v) distances from the pivot point (depicted in A). The model decoupled elastic energy storage and triggering. The moment arm for the torque from the spring is dependent on the geometry of the dactyl and the current state of the dactyl as it closes (inset).

Additionally, we unexpectedly documented a previously unrecognized mechanism for elastic energy storage in snapping shrimp, specifically deformation of the propodus exoskeleton during loading and recoil.

MATERIALS AND METHODS

Animal collection and husbandry

Bigclaw snapping shrimp (*Alpheus heterochaelis* Say 1818) were collected at low tide from oyster reef habitats at the Duke University Marine Lab in Beaufort, NC, USA (NCDENR Scientific and Education permit 707075 to Duke Marine Lab). Filming took place at the Duke University Marine Laboratory or after transport back to the Patek laboratory at the main campus of Duke University in Durham, NC, USA. Individuals were housed in 10.16 cm³ tanks and received partial water changes and frozen krill three times a week. As detailed below, snapping shrimp were filmed during spring loading and snapping. These behaviors were elicited by placing a metal probe or paintbrush near each individual.

Snapping shrimp morphology and mathematical model development

To parameterize the mathematical model with mass, density and length dimensions similar to those of snapping shrimp, we measured snapping shrimp molts using images from a microscope (165M FC microscope; DFC 450 C camera, Leica Microsystems, IL, USA). Based on these measurements, we represented the mathematical model's dactyl as a cylinder with a length of 5.756 mm and width of 1.025 mm. The mass of the modeled dactyl was estimated as 4.750 mg based on the cylinder's volume and water density.

With an additional series of morphological measurements, we further populated the mathematical model with parameters that match the snapping shrimp's geometry and dynamics. We validated prior morphological research (Ritzmann, 1974; Kaji et al., 2018) by visualizing the relative locations of the apodeme (i.e. arthropod tendon) insertion and joint location using dissections and

dye-enhanced micro-computed tomography (micro-CT) scans of fixed claws and molts (Fig. 1; Fig. S1) (XT H 225 ST scanner, Nikon Corp., Tokyo, Japan). The spring attachment point in the model was defined with the assumption that apodeme recoil delivers elastic energy to the dactyl as it rotates around the pivot point. Therefore, we used morphological measurements of the apodeme insertion point relative to the pivot point. Specifically, we measured the horizontal distance (a_h : 1.025 mm) and vertical distance (a_v : 0.264 mm) from the pivot point to the spring attachment point on a snapping shrimp molt (165 mol l⁻¹ FC microscope; DFC 450C camera, Leica Microsystems).

To generate the images in Fig. 1B, a claw was removed from a male specimen and immediately fixed in a 1:1 solution of Bouin's fixative and 100% ethanol for 24 h. The specimen was gradually transferred to 70% ethanol before staining in an iodine solution for 3 days (3:1 70% ethanol:Lugol's solution). The specimen was then micro-CT scanned (125 kV, 80 μ A, voxel size 11.4 μ m, 1518 \times 1393 \times 1514 voxel resolution). For the images in Fig. S1, a dactyl was obtained from a fresh molt, allowed to dry and then scanned (123 kV, 87 μ A, voxel size 12.0 μ m, 1213 \times 1048 \times 923 voxel resolution). CT Pro 3D software (Nikon Corp., Tokyo, Japan) was used to reconstruct each scan. Figure images were generated by AvizoLite 9.5.0 (Thermo Fisher Scientific, Waltham, MA, USA) (Fig. 1B) or OsiriX MD v8.5 (Pixmeo SARL, Geneva, Switzerland) (Fig. S1).

With this morphological information, we developed the mathematical model. The dynamics of the reduced-order model were derived with respect to a global coordinate frame which is attached to the point of rotation of the dactyl (orange circle in Fig. 2). At this fixed pivot point, the mass moment of inertia for the modeled cylindrical dactyl was calculated using the parallel axis theorem as 5.370×10^{-11} kg m². We modeled the dynamic process of latching and unlatching via the torque reversal latch. Our reduced-order model serializes the loading and unlatching processes of the torque reversal latch, such that there are three distinct dynamical states: (1) loading, (2) unlatching and (3) free dactyl movement after

torque reversal (Fig. 1C–E, Fig. 3). Note that the nonstandard coordinate system in the model results in a negative (counterclockwise) torque during opening and loading and a positive (clockwise) torque during closing. Therefore, during loading, a negative torque about the pivot point grows as elastic energy is loaded (blue shaded area Fig. 3). In this dynamical state, the dactyl is stationary because torque is acting in the opening direction. Torque on the dactyl (τ) was calculated as:

$$\tau(\theta) = k_t \sqrt{(2\Delta t(\Delta E/\Delta t)/k_t)} \sqrt{a_h^2 + a_v^2} \sin(\theta_{tr} - (\theta + \theta_{ul})), \quad (1)$$

where the energy loaded to the system is set through energy loading duration (Δt) and energy loading rate ($\Delta E/\Delta t$). k_t is the spring constant of the apodeme. This value is not known for snapping shrimp. We assume that stored elastic energy can be modeled as a single spring with a spring constant of $k_t=5000 \text{ N m}^{-1}$, which is similar to tendon stiffness reported for bullfrogs and similar to the lower range of effective spring constants that have been estimated for arthropod apodeme–cuticular spring systems such as grasshoppers (Rosario et al., 2016). θ_{tr} is the torque reversal angle defined through the arctangent of the ratio of the vertical distance from the pivot to spring attachment point, a_v , to the horizontal distance, a_h [$\theta_{tr}=\text{atan}(a_v/a_h)$]. θ is the angle of the dactyl in the global reference frame. θ_{ul} is the unlatching angle that starts at 0 deg (Fig. 2) and varies with time during unlatching.

Once energy has been fully loaded in the modeled system, the unlatching process begins (red shaded area in Fig. 3). During the unlatching process, spring force rotates through the unlatching angle (θ_{ul}) at the unlatching rate in the direction opposite to the dactyl rotation (Figs 1 and 3). When the sum of the dactyl angle (θ) and unlatching angle (θ_{ul}) is equal to the torque reversal angle (θ_{tr}), then torque (τ) is zero (vertical dashed line in Fig. 3), because the line of action of the spring force goes through the pivot point (Fig. 1D). As soon as the spring force rotates past this point, the torque reverses sign.

After torque reversal, the torque from the spring applied to the dactyl acts in the closing direction and the dactyl moves freely. In addition to accelerating the mass of the dactyl, torque from the spring acts against fluidic drag forces (purple shaded area in Fig. 3). The fluidic drag force is modeled for high Reynolds number regimes, similar to previous mathematical modeling (Tang and Staack, 2019). The equation of motion that governs the dactyl movement is:

$$I \frac{d^2\theta}{dt^2} = \tau(\theta) - \frac{C_D \rho D L^4}{8} \left(\frac{d\theta}{dt} \right)^2, \quad (2)$$

where I is the mass moment of inertia of the dactyl at the pivot point and τ is the torque from the spring element (for full derivation see Appendix and Fig. S1). Drag force on the dactyl was modeled following the approach in Tang and Staack (2019). Specifically, we used the same model that describes the variation in flow velocity along the length of the dactyl. C_D is the drag coefficient (0.5, similar to the modeling in Tang and Staack, 2019), ρ is density of water (1 g cm^{-3}), and D and L are diameter and length of the dactyl, respectively, modeled as a cylinder (as explained in the morphology section above). We computationally modeled the transformation of elastic potential energy to the kinetic energy accelerating the dactyl by continually subtracting the kinetic energy of the dactyl motion from the elastic potential energy in the torque equation.

High-speed imaging of exoskeletal spring deformation

We collected a small dataset to establish exoskeletal deformation in the scientific literature as an additional location of elastic energy storage in this system (previously suspected by Kaji et al., 2018), and to assess the timing of propodus exoskeleton deformation during the loading phase for informing the assumptions of our modeling. To do this, we mounted the claw in place, because the claw normally rotates substantially during a snap, making it difficult to track propodus deformation accurately. Therefore, we affixed a small portion of a toothpick to the dorsal or lateral surface of the propodus and to the posterolateral surface of the carapace with respect to the orientation of the shrimp. This setup immobilized the propodus relative to the body, while allowing the dactyl to rotate freely. The snapping shrimp's body was then attached by a second toothpick to a rig outfitted with micromanipulators so that the claw could be precisely placed within the camera's field of view. Claw deformation was then filmed in the ventral view using the camera and mirror setup described below. We filmed the entire loading phase (30,000–50,400 frames s^{-1} , 18.84–32.33 μs shutter, 896×448 – 1024×688 pixel resolution) and then down-sampled for the digitizing analysis given the slow rate and long duration of loading.

We measured the timing of the start of propodus deformation and percent change in deformation (1 male and 1 female; 4–25 videos per shrimp). We began measuring when the dactyl was cocked in place and ended at the frame when the dactyl first started to close (Fig. 4). We measured the change in distance between two curvatures along the medial and lateral surface of the propodus visible in the ventral view of the videos. We measured the shortest distance between the opposing curvatures for a given frame (Fig. 5A). Each loading video was thresholded in ImageJ (version 1.53f51), such that the edges of the deforming saddles were clearly outlined. Using the DLTdv8a app (version 8.2.5) (Hedrick, 2008) in MATLAB (R2021b, MathWorks, Natick, MA, USA), we measured the change in distance between two curvatures of the propodus from the lateral view starting 30–200 frames before when the dactyl was cocked in place and ending 1–31 frames after the frame when the dactyl first started to snap closed (Movie 1). We calculated the percent change in deformation as the change in length occurring between cocking and snapping divided by the starting (unloaded) length between the two curvatures of the propodus prior to cocking. We used this percent distance as a proxy for propodus deformation such that we could detect the timing of elastic energy storage; this metric does not directly measure the amount or rate of energy stored or the total distribution or location of energy storage in the propodus.

Based on this analysis of propodus deformation (see Results), we established that the duration of dactyl cocking to closing is an effective proxy for duration of elastic loading. Furthermore, measurements of dactyl cocking are feasible in unrestrained kinematics experiments (next section), whereas consistent measurements of the duration and timing of propodus deformation are not possible in less-restrained animals. Therefore, for brevity and congruity with the modeling terminology, when we henceforth refer to snapping shrimp spring loading duration, it is synonymous with the duration between dactyl cocking and first movement of the dactyl in a strike.

High-speed imaging of loading and striking kinematics

In a separate, much larger dataset than that for the propodus deformation analysis, we analyzed loading and snapping of 80 strikes from 8 individuals (6 males, 2 females; 5–13 strikes per individual). Prior to filming, a toothpick was attached to the

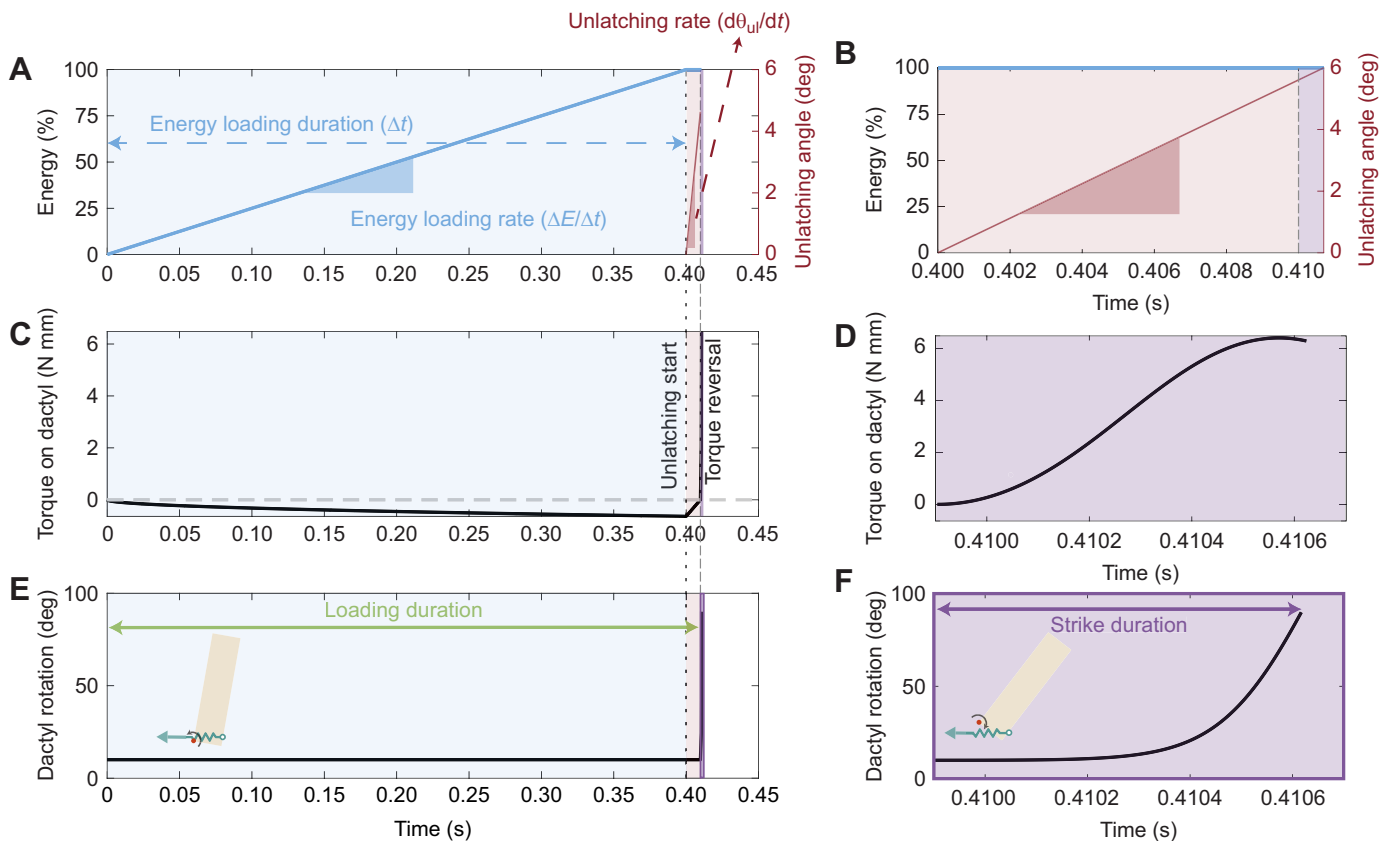


Fig. 3. The actuation, torque and kinematics of the reduced-order model during loading and unlatching. (A) In the reduced-order model, energy is loaded into the system at a linear rate (energy loading rate, $\Delta E/\Delta t$) over a fixed duration of time (energy loading duration, Δt). Once the energy is loaded to the system, unlatching starts at a fixed rate (unlatching rate, $d\theta_{ul}/dt$) and continues until the dactyl rotates to 90 deg. (B) A zoomed-in view of the duration within the dotted region in A to show the energy (blue) and unlatching angle (red) during unlatching and spring actuation. (C) The torque (τ) profile on the dactyl about the pivot point. As energy is loaded to the system, the torque increases in magnitude in the opening direction (negative numbers as per the coordinate system we specified for the model, see Materials and Methods). When energy loading is completed, the torque is at the maximal negative value. As unlatching starts, the torque decreases in magnitude, until reaching zero when the line of action of the spring force is through the pivot point. After rotating past this zero-point, the torque in the system sharply increases while the dactyl rotates to the closed position. (D) A zoomed-in view of duration within the dotted region in C, depicting the torque on the dactyl during spring-actuation. (E) The kinematics of the dactyl rotation (θ) in the model through loading and unlatching. The dactyl is not moving until the system reverses torque. Then, the dactyl quickly rotates closed. (F) A zoomed-in view of the duration within the dotted region in E, showing the kinematics of the simulated dactyl rotation.

dorsoposterior surface of the carapace using a cyanoacrylate adhesive (Loctite^R Super Glue Gel ControlTM) to assist with positioning during filming. We filmed snaps using a high-speed video camera focused on the animal and – in the same field of view – a mirror oriented at 45 deg to the camera’s plane of view. This allowed us to simultaneously visualize two sides of the snapping claw to ensure that we could digitize the view in which the closing of the dactyl was perpendicular to the camera’s view (snapping shrimp readily vary the orientation of their snapping claw relative to their body axis). We filmed snaps with a high-speed video camera (FASTCAM SA-Z type 2100K-M-64GB, Photron, San Diego, CA, USA). Videos were recorded at either 50,400 or 100,000 frames s^{-1} (50,400 frames s^{-1} , 18.84 μs shutter, 640 \times 520 or 896 \times 448 pixel resolution; 100,000 frames s^{-1} , 9.00 μs shutter, 384 \times 408 pixel resolution). These two frame rates were used because smaller individuals strike more quickly, requiring a higher frame rate than the larger individuals. Given the goal of measuring individual variation and reducing variation caused by the experimental setup, we only included videos in the analysis if the claw was oriented <20 deg from horizontal in the lateral view, the video had high contrast and resolution in the ventral view, and the dactyl and bubble

were visible for the entire duration of the strike. For each individual, we only analyzed videos collected within 1 month of the first collected video. Videos were collected in October–November 2018 (5 individuals) or July 2019 (3 individuals).

We measured loading duration beginning at the frame when the dactyl is first fully open and ending with the first frame with visible movement of the dactyl closing. Strike duration was defined as the first frame during which the dactyl begins to close until the frame when the dactyl is fully closed against the propodus (Fig. 4). Given that dactyl morphology constrains the rotation angle and distance traveled by the dactyl during a strike, strike duration is negatively related to strike velocity and acceleration. We digitized points on the dactyl and propodus to determine angular displacement of the dactyl (v 2.0.0, Fiji) (Schindelin et al., 2012). We calculated error (uncertainty) ratios for durations for each individual based on the coarsest high-speed video frame rate used for that individual (Table 2). Note that loading sequences were downsampled from the frame rate used for snapping kinematics, because loading is orders of magnitude longer in duration than snapping. Consequently, loading and snapping data have different measurement uncertainty. Loading duration uncertainty ranged from 0.2% to 3%, and loading

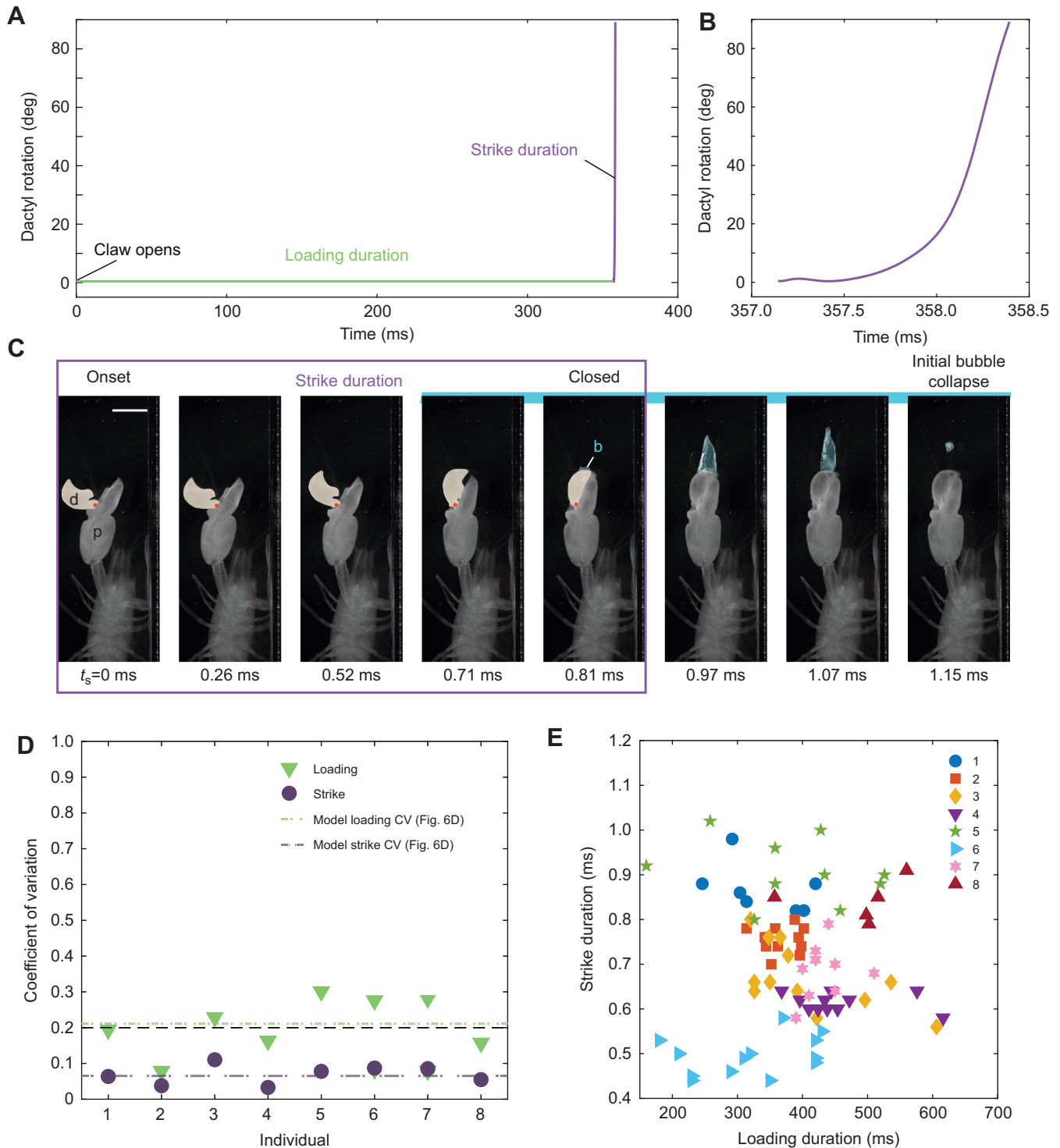


Fig. 4. The extremely short durations of snapping shrimp strikes were stereotyped and not correlated with loading duration. (A) Loading duration, on the order of hundreds of milliseconds, was far greater than strike duration. (B) Strikes occurred in milliseconds. (C) Strike duration began with unlatching (onset), at which point the dactyl (d, tan overlay) rotated around a pivot (orange circle) toward the propodus (p). Just prior to the dactyl fully closing against the propodus, the cavitation bubble (aqua overlay) started to form (0.71 ms; start of horizontal aqua bar) and then collapsed after 1.15 ms. Scale bar: 5 mm. Ventral view with distal toward the top of the page. High speed images were subsampled from the original sequence. (D) The coefficient of variation (CV) for the loading duration (green triangles) was less than that for strike duration (purple circles) for 7 out of 8 individuals. CVs that are less than or equal to 0.20 (black dashed line) have been used to indicate stereotyped movement (Wainwright et al., 2008). For comparison, the loading CV (CV=0.21) and striking CV (CV=0.064) from the model simulations in Fig. 6D are shown as green and purple dashed lines, respectively. (E) Loading and strike duration were not statistically related ($F_{1,71.997}=2.7$, $P=0.104$). Loading duration variation was generally larger than strike duration variation for each individual (colored shapes). A and B depict a different strike from C.

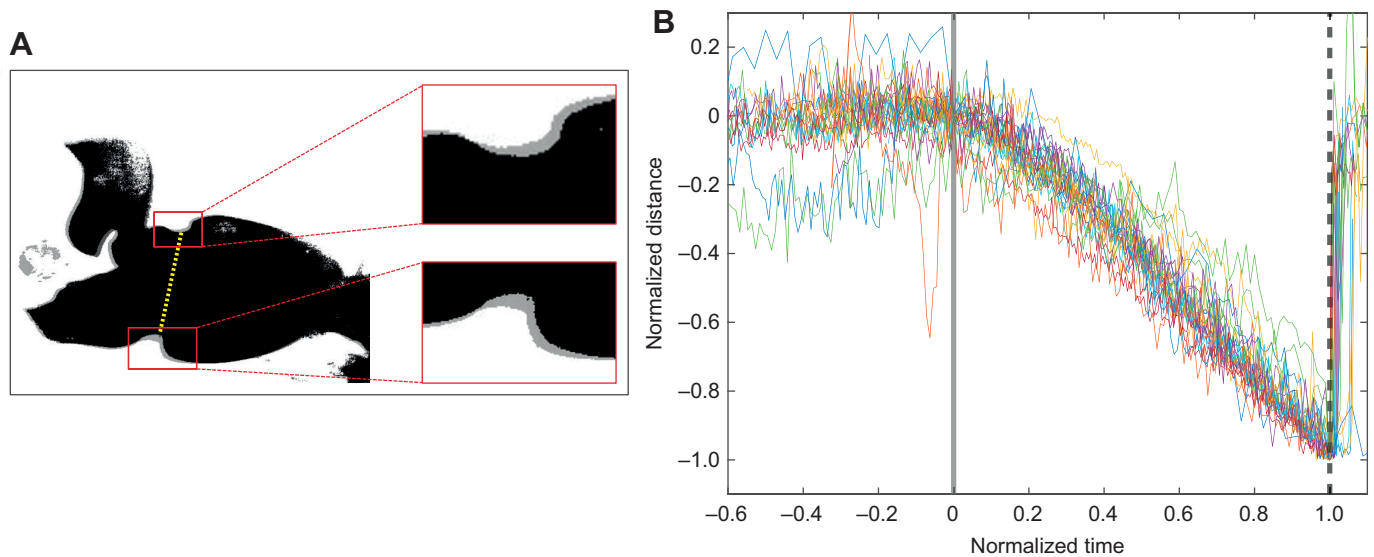


Fig. 5. Deformation of the propodus exoskeleton begins with dactyl opening and recoils once dactyl rotation begins. (A) Video sequences were thresholded to clearly delineate the outline of the propodus as the exoskeleton deformed during elastic loading and release. Distance between two saddle-like regions (red boxes) were tracked. Distal is to the left. Insets: the grayscale image is the starting configuration and the black overlaid image is the fully compressed exoskeleton just prior to dactyl release. The dashed yellow line represents the distance between the two curvatures for the compressed exoskeleton. (B) The shortening distance between the two saddle-shaped regions in A began when the dactyl was fully cocked (gray vertical line). The distance continued to shorten until dactyl release (vertical dashed line), at which point the exoskeleton recoiled back to its original configuration and the rapid snap was launched. Time data were aligned to the onset of dactyl cocking (normalized time zero). Duration was scaled across all sequences such that the duration between dactyl cocking and dactyl release extends from 0 to 1. Likewise, the distance at time zero was aligned to zero and then the total change in distance was scaled from 0 at the dactyl cocking and -1 at dactyl release. Each color represents the tracked distances from a single video.

durations are reported in increments of 1, 2 or 10 ms, depending on the individual. Strike duration uncertainty ranged from 1% to 3%, and strike durations are reported in increments of 0.01 or 0.02 ms, depending on the individual.

We compared variation in loading to variation in strike duration for each individual using the coefficient of variation (CV). The CV is the ratio of standard deviation to the mean and therefore allows for comparison of dispersion when the scales (means) are different. To represent how relative variation decreases or increases between loading and strike durations, we calculated a CV ratio (CVR; strike duration CV divided by loading duration CV). We applied CVR, a novel metric, to compare relative variation in spring loading duration to relative variation in strike duration.

We tested the association between loading duration and strike duration using a linear mixed model with individual ID as a random effect (lmerTest) (Kuznetsova et al., 2017) in R v 3.6.2 (<https://www.r-project.org/>). We used a type III ANOVA with Satterthwaite approximation for degrees of freedom to determine significance.

Simulations

In our first set of simulations, we modeled the mapping of loading duration to strike duration by varying (1) energy loading duration (Δt), (2) energy loading rate ($\Delta E/\Delta t$) and (3) unlatching rate ($d\theta_{ul}/dt$) (defined in Fig. 3A). The energy loading duration and energy loading rate determine the timing and magnitude of elastic energy storage, while the unlatching rate represents the change in the line of action with respect to time. Geometric parameters, such as length, width, pivot and spring locations, were held constant. We defined loading duration as the sum of energy loading duration and duration from the end of energy loading to the start of torque reversal (Fig. 3). Note that this measure of loading duration is defined through events in the model that are not easily measured or apparent in the

biological system, because torque reversal is not visible externally in snapping shrimp.

To parameterize this simulation, we set the mean values of the energy loading duration, energy loading rate and unlatching rate to match the observed results of the high-speed imaging study (loading duration: 409.9 ms, strike duration: 0.7 ms). The dactyl starting angle [$\theta(0)$] was set to 10 deg and the torque reversal angle (θ_{tr}) was set to 15 deg based on the biological measurements. We set standard deviations for each of these parameters such that the CV (the ratio of the standard deviation to the mean) was 20%. Therefore, when we stochastically varied the reduced-order model, each simulation set these parameters from independent draws from normal distributions (energy loading duration: $\mu=392$ ms, $\sigma=89.8$ ms; energy loading rate: $\mu=15$ mJ s $^{-1}$, $\sigma=3$ mJ s $^{-1}$; unlatching rate: $\mu=450$ deg s $^{-1}$, $\sigma=90.0$ deg s $^{-1}$). Note that the mean energy loading duration is smaller than the average loading duration from the high-speed imaging study, because the numerical model measures the loading duration as the duration from the start of the energy loading to the time when the torque reverses sign. In these simulations, we individually perturbed energy loading duration, energy loading rate and unlatching rate, keeping the other two constant at their means. We then simulated the more complex case in which all three parameters could vary simultaneously: each parameter was drawn from the same normal distributions described above, remaining independent from the other two. We stochastically varied these parameters over a total of 400 simulations. Although it is possible that these parameters could be inherently linked in the organism, that scenario was not modeled here.

In a second set of simulations, we tested how the geometry of a torque reversal latch affected strike duration. We varied two parameters: (1) dactyl starting angle [$\theta(0)$] and (2) torque reversal angle (θ_{tr}) (Fig. 2B,C). We simulated distinct combinations of the dactyl starting angle (from 0 to 80 deg) and torque reversal angle

Table 2. Snapping shrimp strike kinematics

	Individual (ID)							
	A5	A11	A13	A15	D001	D002	D003	JD4
No. strikes (<i>n</i>)	7	5	13	10	12	12	11	10
Loading duration								
Coefficient of variation (CV)	0.19	0.16	0.28	0.08	0.08	0.23	0.16	0.30
Mean (ms)	338	487	320	430	366	406	458	382
SD (ms)	66	77	90	30	28	92	74	116
Uncertainty (%)	0.6	0.2	3	2	0.6	0.5	0.4	0.5
Strike duration								
CV	0.06	0.05	0.09	0.09	0.04	0.11	0.03	0.08
Mean (ms)	0.86	0.84	0.50	0.69	0.76	0.68	0.62	1.0
SD (ms)	0.06	0.05	0.04	0.06	0.02	0.08	0.02	0.08
Uncertainty (%)	2	1	2	1	3	3	3	2
CV ratio (CVR)	0.33	0.35	0.32	1.07	0.48	0.48	0.20	0.26

Means, SD, CV and CVR for loading and strike durations for each of the eight individuals in this dataset. CVR is calculated as the strike duration CV divided by the loading duration CV. We calculated error (uncertainty) ratios for loading and strike durations for each individual based on the coarsest high-speed video frame rate used for that individual. Corresponding length and size information can be found in Table S1.

(from 0 to 45 deg) in 1 deg increments. First, we used the average values described above for energy loading duration, energy loading rate and unlatching rate, and then calculated the strike duration at each combination of dactyl starting angle and torque reversal angle. Then, to reduce computation time, we simulated 45 evenly spaced combinations of dactyl starting angle and torque reversal angle. We ran 27 simulations for each combination of angles [$\theta(0)$ and θ_{tr}] in which we varied energy loading duration, energy loading rate and unlatching rate at their respective minimum, mean or maximum values. We calculated the CV as we also did for the biological kinematic data (described above) and then compared the CV between the simulations and snapping shrimp.

All simulations were performed in MATLAB (2018a) using a forward Newton–Euler method with a time step of 1 μ s. Code is available via the Dryad archive for this publication (<https://doi.org/10.5061/dryad.sqv9s4n6k>).

Assumptions and limitations of the model

The goal of our simulations was to generally model the phenomenon of torque reversal latches at similar, generalizable scales as found in LaMSA systems such as the snapping shrimp. We did not aim to explicitly model the snapping shrimp system. Our simulation approach instead aimed to test variation in torque reversal latches to generally understand how and when variation in the kinematic output of a torque reversal latch can occur across a far wider range of variables than might be found in a single biological system.

Therefore, implicit to the model description above, we have made a series of simplifying assumptions in the model, which we outline here. We modeled the dactyl with a simple cylindrical geometry, whereas the snapping shrimp's dactyl has complex morphology that could affect hydrodynamic loading forces on a striking dactyl. We serialized energy loading and unlatching processes to enable simulation of varying inputs, but this does not replicate the likely synchronized process in live snapping shrimp. Given our new discovery of propodus deformation during loading, snapping shrimp likely store elastic energy in both the propodus exoskeleton and apodeme; however, our model assumes (based on previous hypotheses for this mechanism) that elastic energy is delivered to the dactyl solely by recoil of the apodeme at the apodeme attachment location. Therefore, it is possible that in snapping shrimp, like the recently established dual spring force couple mechanism discovered in the trap-jaw ants (Sutton et al.,

2022), the output rotation is even faster given an additional displacement of the pivot by recoiling propodus exoskeleton. However, this possible revision of the elastic mechanism should not change the role of the torque reversal latch and the relative variation of the input and output durations, as we are examining in this simulation. For the same reason, shifts in the modeled stiffness of the elastic mechanism might influence the magnitude of the outputs, but it would not affect the role of the torque reversal latch, which is the focus of our simulations. Finally, we tuned the average model kinematic output to match the average kinematic output of the experimental data, which required free fitting parameters. Consequently, the modeling approach offers limited ability to exactly predict the numerical values of strike duration, velocity or acceleration, such that changing assumptions about geometry, energy loading and unlatching would therefore change the kinematic output of the model.

RESULTS

Exoskeletal deformation

Propodus exoskeletal deformation began as soon as the dactyl was fully opened and continued until the onset of dactyl closure (Fig. 5). Once the dactyl closure began, the deformed propodus exoskeleton recoiled back to its original configuration.

Snapping shrimp strike kinematics

In snapping shrimp, relative variation of strike duration was considerably lower than in loading duration (Fig. 4). Loading duration and strike duration were not correlated ($F_{1,71.997}=2.7$, $P=0.104$). Loading duration ranged from 160 to 616 ms (390 ± 90 ms) (Table 2). Strike duration was much shorter, ranging from 0.44 to 1.02 ms (0.70 ± 0.14 ms). Loading CV ranged from 0.08 to 0.30. Strike CV ranged from 0.03 to 0.11. Strike CV was less than loading CV for 7 out of 8 individuals. Overall, median strike duration CV was significantly lower than median loading duration CV (one-tailed paired Wilcoxon signed rank test: $V=1$, $P=0.008$). Seven individuals had CVRs less than 1 (0.20–0.48), indicating that relative standard deviation of the loading phase was lower by more than half compared with the strike phase. One individual had nearly identical CV values, resulting in a CVR of 1.07.

Simulations

The relationship between loading duration and strike duration was tunable in both of our simulations. In the first simulation, this was

achieved by varying energy loading duration, energy loading rate and unlatching rate individually and in combination. An animation of the model is shown in Movie 3.

Strike duration was less variable ($CV=0.054$) than loading duration ($CV=0.21$) when energy loading duration was varied while fixing both energy loading rate and unlatching rate at their respective means. Loading duration and strike duration CVR was 0.26. Strike duration was inversely related to loading duration (Fig. 6A), because longer loading durations, with a constant energy loading rate, corresponded to more elastic energy in the system and thus shorter strike durations. Varying energy loading rate caused variation in the amount of stored energy, such that strike duration was variable even with a constant loading duration ($CV=0.042$) (Fig. 6B).

Varying unlatching rate was key to tuning the relationship and relative variation between loading and striking duration. Specifically, our simulations demonstrated that when the unlatching rate was exclusively varied, the loading duration and strike duration were both affected (Fig. 6C). Loading duration included both loading duration and unlatching duration until torque reversal (Fig. 3). Varying the unlatching rate caused minimal variation in the loading duration ($CV=0.0053$), and more strongly influenced variation of strike duration ($CV=0.022$, $CVR=4.1$).

When energy loading duration, energy loading rate and unlatching rate were independently and simultaneously varied, loading duration and strike duration were negatively correlated ($F_{1,98}=85.6$, $P=5.13e-15$) (Fig. 6D). Strike duration CV (0.064) was lower than loading duration CV (0.21).

We identified a boundary between latching and non-latching systems. This boundary was revealed by varying latch geometry through simulations of dactyl starting angle [$\theta(0)$] and torque reversal angle (θ_T) (Fig. 7). This boundary (solid black line, Fig. 7A,B) occurred when the difference between dactyl starting angle (Fig. 2B) and torque reversal angle (Fig. 2C) was equal to zero. If the difference between the dactyl starting angle and torque reversal angle was positive, then the dactyl closed through direct actuation of the motor (muscle). Muscle-based actuation was not simulated (white spaces, Fig. 7A,B). When the difference between the dactyl starting angle and torque reversal angle was negative, then spring-actuated motion occurred through the torque reversal latch.

On the side of the boundary when the system was latching, dactyl starting angle and torque reversal angle affected the strike duration. Strike duration ranged from a minimum of 0.58 ms (dactyl starting angle, 45 deg; torque reversal angle, 45 deg) to a maximum of 0.77 ms (dactyl starting angle, 0 deg; torque reversal angle, 0 deg) (Fig. 7A). When the torque reversal angle was held constant, strike duration decreased with increasing dactyl starting angles. A shorter amount of time was needed to close the dactyl, given that the dactyl began in a more closed configuration. When the dactyl starting angle was held constant, the strike duration decreased with increasing torque reversal angle. The increase in torque reversal angle increased the magnitude of the applied torque after the torque reversal event; this caused acceleration of the dactyl and thereby decreased strike duration.

Dactyl starting angle and torque reversal angle influenced the variation in strike duration. Even when using the same set of parameters for loading duration, energy loading rate and unlatching rate, relative variation between loading duration and strike duration were tuned through dactyl starting angle and torque reversal angle. For instance, CVR decreased for dactyl starting angles and torque reversal angles closer to the boundary between latching and non-latching systems. Sets with the same difference between the dactyl

starting angle and torque reversal angle had the same CVR. Greater differences between dactyl starting angle and torque reversal angle corresponded to a higher CVR. For example, a dactyl starting angle of 0 deg and torque reversal angle of 5 deg (a difference of -5 deg) had a CVR of 0.33, and a dactyl starting angle of 40 deg and torque reversal angle of 45 deg (a difference of -5 deg) also had a CVR of 0.33. A more extreme example of a simulation with a dactyl starting angle of 0 deg and torque reversal angle of 45 deg (a difference of -45 deg) yielded a CVR of 0.40. With these configurations, relatively more variation occurs in strike duration even though the respective simulations use the same set of energy loading durations, energy loading rates and unlatching rates.

The simulated 'individual' from Fig. 6 has a dactyl starting angle and torque reversal angle closer to the boundary between latching and non-latching systems than the rest of the simulated data. We plotted the simulation results from Fig. 6D as a single circular marker in Fig. 7B. This marker has a relatively low CVR of 0.30 (dark blue).

Comparison of simulations and snapping shrimp kinematics

Compared with our snapping shrimp kinematics dataset, our simulations yielded a stereotyped strike duration (CV , 0.064; CVR , 0.30; Fig. 6D); note that these simulations are based on a different geometry than in Fig. 7). The range of loading durations from the model was similar to those observed from snapping shrimp (Fig. 6D).

DISCUSSION

Our integrated approach of collecting a large kinematic dataset from snapping shrimp and developing a reduced-order model to simulate the effects of small geometric changes to torque reversal latches revealed multiple insights about the role of geometric latches in spring-propelled systems. In snapping shrimp, the torque reversal latch plays a key role in reducing the effect of variation that occurs during spring loading on the strike kinematics. Even so, small adjustments to the torque reversal system as expressed in the model reveal a boundary between spring-driven and muscle-driven configurations, and between an ability to vary kinematic output or nearly eliminate variation in kinematic output. As we discuss below, our study offers a new lens through which to view the elastic mechanism in snapping shrimp, a quantitative comparative framework for the role of geometric latches in biology, and a new framework for using small shifts in geometry to enable control of ultrafast systems in biology and engineering.

Elastic mechanism in snapping shrimp

We established that snapping shrimp deform their propodus exoskeleton during spring loading and that the exoskeleton recoils when the dactyl rotation begins. Spring loading occurs throughout the time period between dactyl cocking and release (Fig. 5). This type of exoskeletal elastic loading is consistent with mechanisms used by other arthropods with LaMSA mechanisms (Patek et al., 2004, 2007; Zack et al., 2009; Burrows and Sutton, 2012; Patek et al., 2013; Rosario and Patek, 2015; Larabee et al., 2017; Patek, 2019; Sutton et al., 2022). To our knowledge, propodus deformation as an elastic mechanism has not been previously established in snapping shrimp.

Given that the dactyl is not closing while the propodus is deforming, elastic energy is likely stored both through the visible exoskeletal deformation and stretching of the internal apodeme. Therefore, our measurements of loading duration encompass the maximum duration for elastic energy storage, as well as unlatching

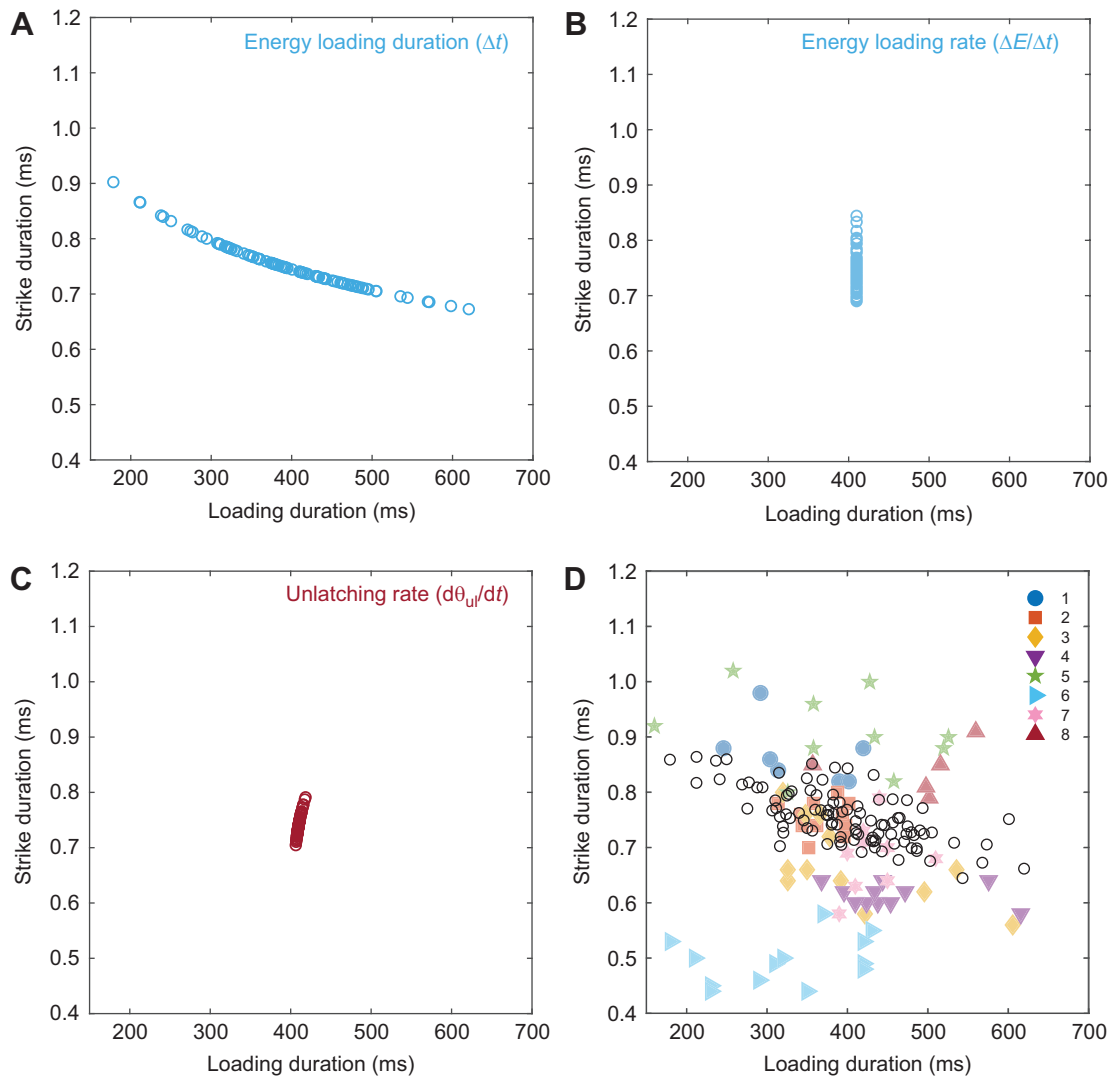


Fig. 6. Torque reversal latch mechanics reduced variation in strike duration under variable actuation in both the reduced-order model and the biological dataset. We simulated the individual and combined effects of varying energy loading duration, energy loading rate and unlatching rate. (A) Greater loading duration increased stored elastic energy and higher strike kinetic energy, which decreased strike duration. (B) Simulated loading durations were equivalent, but strike durations varied because elastic energy was loaded at different rates. (C) Simulated loading duration was affected by unlatching rate, because loading duration was defined as the sum of energy loading duration and the time to torque reversal. (D) When simulated loading duration, loading rate and unlatching rate were varied simultaneously and independently, loading and strike durations from the simulations (open circles) exhibited similar variance in loading duration, but not strike duration, as the biological dataset (transparent colored symbols, from Fig. 4E). For all plots, the reduced-order model was varied stochastically, 100 simulations for each plot, by perturbing loading duration, loading rate and unlatching rate. Loading duration (A), energy loading rate (B) and unlatching rate (C) were sampled from a normal distribution with the mean tuned to the experimental results of snapping shrimp kinematics with standard deviation set as 20% of the mean.

duration and any additional processes that occur prior to the observed onset of the striking motion (e.g. delays owing to dactyl inertia).

Consistent with the timing of propodus deformation, prior research demonstrated that activity of the main spring loading muscle (Cl_1) begins immediately after the dactyl opens, and that activity of this muscle overlaps with trigger muscle (τ) activity prior to dactyl closure (Fig. 1) (Ritzmann, 1974). Deformation of the propodus during the loading phase validates that the muscles inside the propodus are indeed active during this period; propodus shape deformation most likely occurs owing to Cl_1 muscle activity compressing the propodus exoskeleton while the dactyl is latched (although trigger muscle activity could also contribute).

The discovery of propodus deformation in snapping shrimp may point toward their use of a dual spring force couple, as was recently discovered in trap-jaw ants (Sutton et al., 2022). Dual spring force couples in LaMSA systems are formed by combination of a recoiling apodeme and deformation of exoskeleton to develop torque on rotating spring-propelled systems. Although it is not yet clear where the recoiling propodus exoskeleton would develop torque in snapping shrimp, one possibility is that the recoil pushes the dactyl's pivot distally. This would cause the dactyl to rotate even more quickly than predicted by our model (our mathematical model only incorporates apodeme recoil to power the dactyl's rotation). As addressed in the Materials and Methods, this possible new mechanism for spring propulsion in snapping shrimp is worthy of further study but should not substantially change the conclusions of

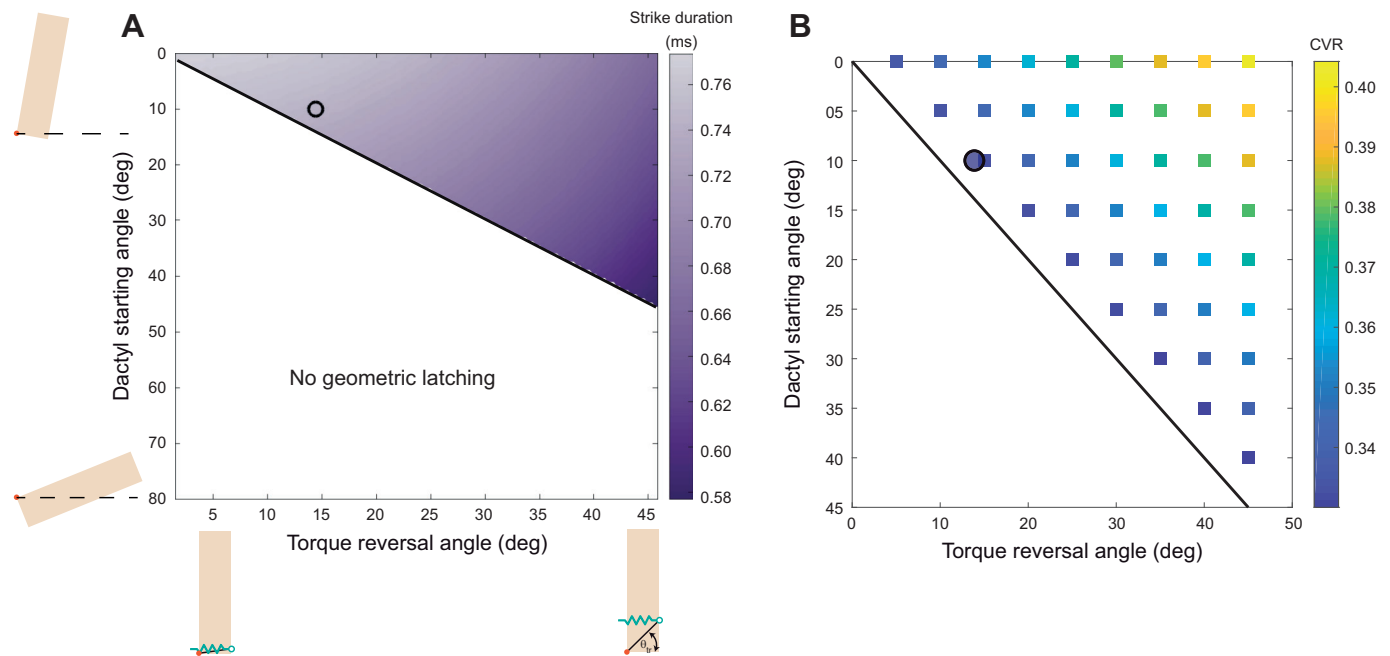


Fig. 7. Geometry of the torque reversal latch changed the relative variation of the strike, given the same stochastic spring loading. The black circle in both panels indicates the configuration used in the simulations depicted in Fig. 6. (A) While keeping energy loading duration, energy loading rate and unlatching rate fixed, we simulated the effect of varying dactyl starting angle and torque reversal angle on strike duration (see Fig. 2 and Table 1 for definitions). The blank region indicates the configurations for a non-latching system, in which the dactyl closes through muscle contraction, not spring propulsion. When a torque reversal latch was present (purple region), the dactyl starting angle and torque reversal angle affected strike duration. With a smaller dactyl starting angle, strike duration was inherently decreased (lighter purple). When the torque reversal angle was larger, strike duration decreased. (B) Energy loading duration, energy loading rate and unlatching rate were each varied independently of each other for a total of 27 simulations per square marker. The resulting variation in strike duration was calculated using the coefficient of variation ratio (CVR). CVR decreased with increasing proximity to the boundary with no latching (black line) (CVR=0.33). With increasing distance from the latching boundary, CVR increased, meaning that variation in energy loading duration, energy loading rate and unlatching rate had a greater effect on strike duration.

the present study. Our model was developed to test the role of torque reversal on tuning the relative variability of spring loading and strike duration, and the model was not structured to predict strike velocity for a specific system.

Torque reversal latches

We found that, in addition to their role in geometrically mediating the onset of movement as a latch in LaMSA systems (Steinhardt et al., 2021), torque reversal latches also can mediate the magnitude and relationship between input and output variation. Our mathematical model reveals how torque reversal latches confer substantial tunability of the correlation and relative variation between loading and strike durations. By structuring the model to serialize energy loading and unlatching processes of the torque reversal mechanism, we were able to simulate and test how independent change of each process affects loading and strike duration. Our use of a reduced-order model allows us to characterize variability in the dynamics of torque reversal latches in general, similarly to the template and anchor approach in legged locomotion (Full and Koditschek, 1999). The ability of the torque reversal latch simulated here to manipulate the relative variation between loading and strike phases has important implications for robust and repeatable biological and synthetic systems, especially considering that this form of control can be implemented mechanically through latch design (Koh et al., 2015; Steinhardt et al., 2021). The question of whether all latches (e.g. contact, fluidic) or even other geometric latches (e.g. mechanical advantage) similarly attenuate input to output variation is an exciting avenue for future research (Hyun et al., 2023). This is particularly interesting

for synthetic design when considering trade-offs between the demands of high performance with output tunability.

The reduced-order modeling approach allows hypothesis testing about the torque reversal mechanism and the effects on performance when perturbing individual actuation parameters that govern elastic energy loading and energy mediation during unlatching (Fig. 3). Simultaneously and independently allowing energy loading duration, energy loading rate and unlatching rate to vary produces output with similar levels of variation as within individuals in the biological data (Fig. 6D). However, the simulated data show a slight negative correlation between loading duration and strike duration that is not seen in the biological data. Note that the simulations in Fig. 6D represent many samples from a single ‘individual’ (a fixed set of geometric parameters), while the spread of the biological samples along the y-axis is attributable in part to individual variation (e.g. animal size). Overall, the simulations suggest that variation in input actuation could account for the variability in loading duration observed in snapping shrimp. Given that muscle activity is not visible in the high-speed videos and is known to vary in other LaMSA systems (Lappin et al., 2006; Kagaya and Patek, 2016), snapping shrimp also likely vary the muscle contractions responsible for energy storage and unlatching.

Although sequential actuation in our model is insightful, it is important to note that many biological and synthetic systems may not have independent control over spring loading and triggering unlatching to allow for tunability. Moreover, the actuators (e.g. muscle) responsible for spring loading and triggering will have their own dynamics. For instance, in snapping shrimp, the trigger muscle activation overlaps with loading muscle activity (Ritzmann, 1974).

Similarly, in a previously developed ‘flea robot’ that used a torque reversal latch, the actuators for energy storage and unlatching are coupled through the circuitry and thus are temporally linked (Noh et al., 2012). If any of the actuation parameters are coupled, we would expect overall less variation in both our input and output timing measurements. The pathways by which variation decreases would be a result of both how the actuation parameters are coupled, as well as their inherent actuator dynamics, where transient dynamics of actuators (e.g. muscles) would affect timing in loading and the system unlatching. For example, in our model, setting the unlatching to always start when a force threshold is reached, analogous to an adhesive latch, would result in a decrease in variation in both loading duration and strike duration. Such an adjustment would apply to other snapping shrimp species in which adhesive discs play a more significant role in latching (Ritzmann, 1973; Ritzmann, 1974).

Our simulations suggest a generalized principle of torque reversal systems such that biological systems can evolve torque reversal systems that either reduce or enhance variable outputs. Our large high-speed video dataset reveals a stark contrast between the high magnitude and variability of the loading duration and the low variation of strike duration in the snapping shrimp *A. heterochaelis*, without a significant relationship between loading and strike duration across individuals. The reduced-order model for the torque reversal latch allowed us to evaluate the role of the latch in producing these biological observations. We found that for a fixed set of geometric parameters similar to an individual of this species, the system can achieve a stereotyped output relative to input. Therefore, torque reversal latches can attenuate variation by their fundamental dynamics, reducing the magnitude of variation of the outputs relative to the inputs, and allowing for relatively stereotyped outputs even with perturbations during spring loading and actuation.

Pathways to geometric latches that amplify mechanical power and attenuate variation

Our work demonstrates how subtle changes in geometry mark a transition from non-latching to latching systems with rapid, highly stereotyped output (Fig. 7). We explored the consequences of two adjustments: dactyl starting angle and the torque reversal angle, which represents the attachment point of the spring relative to the pivot point. We found that these two adjustments influence the presence/absence of a torque reversal latch, vary strike duration, and change the relative variation between energy loading duration, energy loading rate and unlatching rate to the strike duration (represented by the CVR between loading and strike duration).

When torque reversal latches are near the boundary at which a latch would no longer be present, they have the lowest CVRs. In other words, torque reversal latches with these specific parameters attenuate variation contributing to output stereotypy, while configurations with parameters farther from this boundary could have more control of strike output. Our results also demonstrate that geometric parameter pairs that are parallel to the boundary line have equal CVRs and affect the magnitude and relationship of input and output variation owing to their similar dynamics, despite differences in the magnitude of strike durations (Fig. 7B).

Seemingly small changes in dactyl morphology result in the sudden transition from a directly actuated dactyl to one with a spring-driven, torque reversal latch (Fig. 7). This transition mirrors a similar boundary for a flea-inspired robot with a torque reversal

mechanism (Noh et al., 2012) and reflects similar dynamics of latch release and energy flow in mantis shrimp (Patek, 2019; Steinhardt et al., 2021). The stark boundary is characteristic of a system in which relatively small changes in certain aspects of morphology (but not others) can generate seemingly disproportionate jumps in performance (Koehl, 1996; Anderson and Patek, 2015; Muñoz et al., 2018). Torque reversal latches have evolved multiple times in snapping shrimp (Kaji et al., 2018; Chow et al., 2021), and our simulation hints at how sensitivity to small changes in joint or pivot morphology would allow organisms to transition across the non-latching to latching boundary. Indeed, joint and apodeme/tendon insertion positions that are nearly aligned may act as preadaptations for geometric latches.

Benefits of a torque reversal latch for biology and engineering

The ability to vary movement in response to a specific situation or stimulus can increase performance. However, given the rapid speed and short durations of LaMSA movements (Sakes et al., 2016; Ilton et al., 2018), responding to changing stimuli can be difficult or impossible using neuromuscular feedback loops (Hyun et al., 2023). This, in turn, seems to be at odds with the fact that snapping shrimp can produce rapid, cavitation-inducing dactyl closure in diverse environmental and behavioral contexts. Here, we found that mechanical features of the underlying components play important roles in determining input-output responses. Considering the difficulty of generating cavitation in water, the torque reversal latch in snapping shrimp may mitigate small differences in loading and triggering energetics while still allowing for stereotyped, short-duration, high-energy dactyl closure to occur. Latch geometry similar to *A. heterochaelis* resides near the transition between latching and non-latching morphology (Fig. 7), where the attenuation of input to output variation is expected to be strongest. A morphological configuration that attenuates variation from the input to a stereotyped output could compensate for perturbations in inputs, including from changes in the muscle dynamics over repeated use or from fluctuations in the environment itself. The torque reversal latch also allows control over the onset of impulsive movement (Steinhardt et al., 2021), potentially allowing organisms to spend variable amounts of time aiming, reorienting, sensing or bracing for an imminent strike, without compromising output (Crane et al., 2018). This has important implications for trait evolution and mechanical sensitivity (Muñoz et al., 2017, 2018; Muñoz, 2019), while also demonstrating that evolutionary transitions to torque reversal latches may be favored when there is a need to be flexible in the face of uncertain conditions, while maintaining consistent output.

Latches can ultimately dictate the control authority over output performance by geometrically mediating variation and coupling across energy input and kinematic output (Hyun et al., 2023). For example, an engineered LaMSA with a torque reversal latch may be able to produce a stereotyped output under a variety of conditions from the predictable mechanics of the latch itself, which alleviates the need for ‘on-board’ sensing and processing, especially for size- and resource-constrained systems (St. Pierre and Bergbreiter, 2019). Conversely, latch geometry can attenuate variation from imperfect manufacturing or actuation, reducing a need for active control to produce a consistent output. Manufacturing tolerances can have a significant effect on mechanisms such as springs as the engineered system decreases in size (Caro et al., 2005; Dieter and Schmidt, 2012). When using springs with relatively large tolerances for

actuation, a torque reversal latch with predictable mechanics presents a significant pathway for tuning, enhancing or reducing variability in pre-loaded elastic mechanisms found in both biological and engineered LaMSA systems.

Appendix

The reduced-order model was derived with respect to a global coordinate frame that is attached to the point of rotation of the dactyl (orange circle in Fig. 2). Deriving the equation of motion for the one degree-of-freedom rotation system using a Newtonian mechanics approach requires the mass moment of inertia of the rotating body and the torques acting on the body. First, the mass moment of inertia of the cylinder is calculated as:

$$I = I_{\text{cm}} + m \left(\left(\frac{L}{2} \right)^2 + \left(\frac{a_h}{2} \right)^2 \right), \quad (\text{A1})$$

where I_{cm} is the mass moment of inertia at the center of a cylinder ($I_{\text{cm}} = \frac{m}{12} L^2$), and m is mass of the dactyl.

Next, the torque applied by the spring needs to be represented as an equation and is a function of the geometry of the model and the current state of the model. In general, a torque is the product of a force by a moment arm ($\tau = F \times d$). In the case of our model the force is from the spring (teal spring in Figs 2 and 3A), and the moment arm is the perpendicular distance from the point of rotation of the dactyl (filled orange circle in Fig. 2) to the line of action of the spring. The force is calculated from the spring constant and deformation of the spring ($F = k_t \delta$). However, the deformation is not explicitly measured and modeled, and is calculated from the loaded energy $[\Delta t \left(\frac{\Delta E}{\Delta t} \right)]$ as:

$$\delta = \sqrt{\frac{2\Delta t \left(\frac{\Delta E}{\Delta t} \right)}{k_t}}, \quad (\text{A2})$$

and the force is then equal to:

$$F = k_t \sqrt{\frac{2\Delta t \left(\frac{\Delta E}{\Delta t} \right)}{k_t}}. \quad (\text{A3})$$

Next, the moment arm (d) needs to be defined in terms of the system parameters and current state of the model. Fig. 2C shows the moment arm as a dashed line and defines an internal angle. The moment arm is then:

$$d = \sqrt{a_h^2 + a_v^2} \sin(\theta_{\text{tr}} - (\theta + \theta_{\text{ul}})). \quad (\text{A4})$$

Using Eqns A3 and A4, the torque is then equal to:

$$\tau(\theta) = k_t \sqrt{\left(2\Delta t \left(\frac{\Delta E}{\Delta t} \right) / k_t \right)} \sqrt{a_h^2 + a_v^2} \sin(\theta_{\text{tr}} - (\theta + \theta_{\text{ul}})). \quad (\text{A5})$$

The only modeled torque acting against the dactyl is from the drag force from the surrounding fluid. This is modeled similarly to Tang and Staack (2019) as a lumped approximation of the flow velocity

along the length of the dactyl. The drag torque (τ_{drag}) is:

$$\tau_{\text{drag}} = \int_0^L C_D \frac{1}{2} \rho \left(\frac{d\theta}{dt} \right)^2 l^3 D dl = \frac{C_D \rho D L^4}{8} \left(\frac{d\theta}{dt} \right)^2, \quad (\text{A6})$$

where the torque is integrated along the length of the dactyl and l is the length coordinate along the dactyl.

And the full, one degree-of-freedom equation of motion is:

$$I \frac{d^2\theta}{dt^2} = \tau(\theta) - \frac{C_D \rho D L^4}{8} \left(\frac{d\theta}{dt} \right)^2. \quad (\text{A7})$$

Acknowledgements

We are grateful to members of our Impulsive MURI team, Patek Lab and Bergbreiter Lab for helpful feedback on this research. We also thank those who helped with animal collection, filming, animal care and digitizing, especially W. Ray, G. Farley, J. Dinh, S. Hanson, G. Pentapalli, A. Lin and M. Huang.

Competing interests

The authors declare no competing or financial interests.

Author contributions

Conceptualization: S.J.L., R.S., S.B., S.C., B.S., S.N.P.; Methodology: S.J.L., R.S., S.B., S.C., B.S., S.N.P.; Software: S.J.L., R.S., S.C., S.N.P.; Validation: S.J.L., R.S.; Formal analysis: S.J.L., R.S., S.C., B.S., S.N.P.; Investigation: S.J.L., R.S., B.S., S.N.P.; Resources: R.S., S.B., S.N.P.; Data curation: S.J.L., R.S., S.C., B.S., S.N.P.; Writing - original draft: S.J.L., R.S., S.N.P.; Writing - review & editing: S.J.L., R.S., S.B., S.C., B.S., S.N.P.; Visualization: S.J.L., R.S., S.C., B.S., S.N.P.; Supervision: S.N.P.; Project administration: S.B., S.N.P.; Funding acquisition: S.B., S.N.P.

Funding

This work was supported by the U.S. Army Research Laboratory and the U.S. Army Research Office under contract/grant number W911NF-15-1-0358. This work was performed in part at the Duke University Shared Materials Instrumentation Facility (SMIF), a member of the North Carolina Research Triangle Nanotechnology Network (RTNN), which is supported by the National Science Foundation (award number ECCS-2025064) as part of the National Nanotechnology Coordinated Infrastructure (NNCI).

Data availability

Data and MATLAB and R scripts are available at Dryad (Patek et al., 2023): <https://doi.org/10.5061/dryad.sqv9s4n6k>

References

- Abbott, E. M., Nezwik, T., Schmitt, D. and Sawicki, G. S. (2019). Hurry up and get out of the way! Exploring the limits of muscle-based latch systems for power amplification. *Integr. Comp. Biol.* **59**, 1546-1558. doi:10.1093/icb/icz141
- Aguilar, J., Lesov, A., Wiesenfeld, K. and Goldman, D. I. (2012). Lift-off dynamics in a simple jumping robot. *Phys. Rev. Lett.* **109**, 174301. doi:10.1103/PhysRevLett.109.174301
- Alam, P., Sanka, I., Alam, L. P., Wijaya, S., Sintya, E., Handayani, N. S. N. and Rivero-Müller, A. (2018). The snapping shrimp dactyl plunger: a thermomechanical damage-tolerant sandwich composite. *Zoology* **126**, 1-10. doi:10.1016/j.zool.2017.11.001
- Amini, S., Tadayan, M., Chua, J. Q. I. and Miserez, A. (2018). Multi-scale structural design and biomechanics of the pistol shrimp snapper claw. *Acta Biomater.* **73**: 449-457. doi:10.1016/j.actbio.2018.04.038
- Anderson, P. S. L. and Patek, S. N. (2015). Mechanical sensitivity reveals evolutionary dynamics of mechanical systems. *Proc. R. Soc. B* **282**, 20143088. doi:10.1098/rspb.2014.3088
- Armour, R., Paskins, K., Bowyer, A., Vincent, J. and Megill, W. (2007). Jumping robots: a biomimetic solution to locomotion across rough terrain. *Bioinspir. Biomim.* **2**, S65-S82. doi:10.1088/1748-3182/2/3/S01
- Beal, B. F. (1983). Predation of juveniles by the hard clam *Mercenaria mercenaria* (Linne) by the snapping shrimp *Alpheus heterochaelis* Say and *Alpheus normanni* Kingsley. *J. Shellfish Res.* **3**, 1-9. doi:10.2983/035.037.0101
- Bennet-Clark, H. C. (1975). The energetics of the jump of the locust *Schistocerca gregaria*. *J. Exp. Biol.* **63**, 53-83. doi:10.1242/jeb.63.1.53
- Bennet-Clark, H. C. and Lucey, E. C. A. (1967). The jump of the flea: a study of the energetics and a model of the mechanism. *J. Exp. Biol.* **47**, 59-76. doi:10.1242/jeb.47.1.59

- Bolmin, O., Wei, L., Hazel, A. M., Dunn, A. C., Wissa, A. and Alleyne, M.** (2019). Latching of the click beetle (Coleoptera: Elateridae) thoracic hinge enabled by the morphology and mechanics of conformal structures. *J. Exp. Biol.* **222**, jeb196683. doi:10.1242/jeb.196683
- Bolmin, O., Socha, J. J., Alleyne, M., Dunn, A. C., Fezzaa, K. and Wissa, A. A.** (2021). Nonlinear elasticity and damping govern ultrafast dynamics in click beetles. *Proc. Natl. Acad. Sci. USA* **118**: e2014569118. doi:10.1073/pnas.2014569118
- Burrows, M.** (2009). How fleas jump. *J. Exp. Biol.* **212**, 2881-2883. doi:10.1242/jeb.022855
- Burrows, M. and Morris, O.** (2003). Jumping and kicking in bush crickets. *J. Exp. Biol.* **206**, 1035-1049. doi:10.1242/jeb.00214
- Burrows, M. and Sutton, G. P.** (2012). Locusts use a composite of resilin and hard cuticle as an energy store for jumping and kicking. *J. Exp. Biol.* **215**, 3501-3512. doi:10.1242/jeb.071993
- Caro, S., Bennis, F. and Wenger, P.** (2005). Tolerance synthesis of mechanisms: a robust design approach. *J. Mech. Des.* **127**, 86-94. doi:10.1115/1.1825047
- Chow, L. H., De Grave, S., Anker, A., Poon, K. K. Y., Ma, K. Y., Chu, K. H., Chan, T.-Y. and Tsang, L. M.** (2021). Distinct suites of pre- and post-adaptations indicate independent evolutionary pathways of snapping claws in the shrimp family Alpheidae (Decapoda: Caridea). *Evolution* **72**, 2898-2910. doi:10.1111/evo.14351
- Crane, R. L., Cox, S. M., Kisare, S. A. and Patek, S. N.** (2018). Smashing mantis shrimp strategically impact shells. *J. Exp. Biol.* **221**, jeb176099. doi:10.1242/jeb.176099
- Dieter, G. and Schmidt, L.** (2012). *Engineering Design*. New York, NY: McGraw-Hill Education.
- Dinh, J. P.** (2022). Large and exaggerated sexually selected weapons comprise high proportions of metabolically inexpensive exoskeleton. *Biol. Lett.* **18**, 20210550. doi:10.1098/rsbl.2021.0550
- Dinh, J. P. and Patek, S. N.** (2022). Weapon performance and contest assessment strategies of the cavating snaps in snapping shrimp. *Funct. Ecol.* doi:10.1111/1365-2435.14190
- Dinh, J. P. and Radford, C.** (2021). Acoustic particle motion detection in the snapping shrimp (*Alpheus richardsoni*). *J. Comp. Physiol. A* **207**, 641-655. doi:10.1007/s00359-021-01503-4
- Dinh, J. P., Azza, J. and Patek, S. N.** (2020). Winner effects and switching assessment strategies facilitate fast and frugal decisions in territorial contests. *Anim. Behav.* **170**, 189-205. doi:10.1016/j.anbehav.2020.09.012
- Divi, S., Ma, X., Ilton, M., St. Pierre, R., Eslami, B., Patek, S. N. and Bergbreiter, S.** (2020). Latch-based control of energy output in spring actuated systems. *J. R. Soc. Interface* **17**, 20200070. doi:10.1098/rsif.2020.0070
- Full, R. J. and Koditschek, D. E.** (1999). Templates and anchors: neuromechanical hypotheses of legged locomotion on land. *J. Exp. Biol.* **202**, 3325-3332. doi:10.1242/jeb.202.23.3325
- Galantis, A. and Woledge, R.** (2003). The theoretical limits to the power output of a muscle-tendon complex with inertial and gravitational loads. *Proc. R. Soc. B* **270**, 1493-1498. doi:10.1098/rspb.2003.2403
- Gorb, S. N.** (2004). The jumping mechanism of cicada *Cercopis vulnerata* (Auchenorrhyncha, Cercopidae): skeleton-muscle organisation, frictional surfaces, and inverse-kinematic model of leg movements. *Arthropod. Struct. Dev.* **33**, 201. doi:10.1016/j.asd.2004.05.008
- Gronenberg, W.** (1996). Fast actions in small animals: springs and click mechanisms. *J. Comp. Physiol. A* **178**, 727-734. doi:10.1007/BF00225821
- Hedrick, T.** (2008). Software techniques for two- and three-dimensional kinematic measurements of biological and biomimetic systems. *Bioinspir. Biomim.* **3**, 1-6. doi:10.1088/1748-3182/3/3/034001
- Heitler, W. J.** (1974). The locust jump: specialisations of the metathoracic femoral-tibial joint. *J. Comp. Physiol.* **89**, 93-104. doi:10.1007/BF00696166
- Herberholz, J. and Schmitz, B.** (1999). Flow visualisation and high speed video analysis of water jets in the snapping shrimp (*Alpheus heterochaelis*). *J. Comp. Physiol. A* **185**, 41-49. doi:10.1007/s003590050364
- Hughes, M.** (1996a). The function of concurrent signals: visual and chemical communication in snapping shrimp. *Anim. Behav.* **52**, 247-257. doi:10.1006/anbe.1996.0170
- Hughes, M.** (1996b). Size assessment via a visual signal in snapping shrimp. *Behav. Ecol. Sociobiol.* **38**, 51-57. doi:10.1007/s002650050216
- Hyun, N. P., Olberding, J. P., De, A., Divi, S., Liang, X., Thomas, E., St. Pierre, R., Steinhardt, E., Jorge, J., Longo, S. J. et al.** (2023). Spring and latch dynamics can act as control pathways in ultrafast systems. *Biomim. Bioinspir.* **18**, 026002. doi:10.1088/1748-3190/acaa7c
- Ilton, M., Bhamla, M. S., Ma, X., Cox, S. M., Fitchett, L. L., Kim, Y., Koh, J.-., Krishnamurthy, D., Kuo, C.-Y., Temel, F. Z. et al.** (2018). The principles of cascading power limits in small, fast biological and engineered systems. *Science* **360**, eaao1082. doi:10.1126/science.aao1082
- Kagaya, K., Patek, S. N.** (2016). Feed-forward motor control of ultrafast, ballistic movements. *J. Exp. Biol.* **219**, 319-333. doi:10.1242/jeb.130518
- Kaji, T., Anker, A., Wirkner, C. S. and Palmer, A. R.** (2018). Parallel saltational evolution of ultrafast movements in snapping shrimp claws. *Curr. Biol.* **28**, 106-113.e4. doi:10.1016/j.cub.2017.11.044
- Kallal, R. J., Elias, D. O. and Wood, H. M.** (2021). Not so fast: strike kinematics of the araneoid trap-jaw spider *Pararchaea alba* (Malkaridae: Pararchaeinae). *Integr. Org. Biol.* **3**, obab027. doi:10.1093/iob/obab027
- Kingston, A. C. N., Woodin, S. A., Wethey, D. S. and Speiser, D. I.** (2022). Snapping shrimp have helmets that protect their brains by dampening shock waves. *Curr. Biol.* **32**, 3576-3583.e3. doi:10.1016/j.cub.2022.06.042
- Knowlton, N. and Keller, B. D.** (1982). Symmetric fights as a measure of escalation potential in a symbiotic, territorial snapping shrimp. *Behav. Ecol. Sociobiol.* **10**, 289-292. doi:10.1007/BF00302819
- Koehl, M. A. R.** (1996). When does morphology matter? *Annu. Rev. Ecol. Syst.* **27**, 501-542. doi:10.1146/annurev.ecolsys.27.1.501
- Koh, J.-S., Yang, E., Jung, G.-P., Yang, E., Jung, S.-P., Son, J., Lee, S., Jablonski, P. G., Wood, R. J., Kim, H.-Y. et al.** (2015). Jumping on water: surface tension-dominated jumping of water striders and robotic insects. *Science* **349**, 517-521. doi:10.1126/science.aab1637
- Koukouvini, P., Bruecker, C. and Gavaises, M.** (2017). Unveiling the physical mechanism behind pistol shrimp cavitation. *Sci. Rep.* **7**, 13994. doi:10.1038/s41598-017-14312-0
- Kuznetsova, A., Brockhoff, P. B. and Christensen, R. H. B.** (2017). lmerTest package: tests in linear mixed effects models. *J. Stat. Softw.* **82**, 1-26. doi:10.18637/jss.v082.i13
- Lappin, A. K., Monroy, J. A., Pilarski, J. Q., Zepnewski, E. D., Pierotti, D. J. and Nishikawa, K. C.** (2006). Storage and recovery of elastic potential energy powers ballistic prey capture in toads. *J. Exp. Biol.* **209**, 2535-2553. doi:10.1242/jeb.02276
- Larabee, F. J., Gronenberg, W. and Suarez, A. V.** (2017). Performance, morphology and control of power-amplified mandibles in the trap-jaw ant *Myrmoterax* (Hymenoptera: Formicidae). *J. Exp. Biol.* **220**, 3062-3071. doi:10.1242/jeb.156513
- Lohse, D., Schmitz, B. and Versluis, M.** (2001). Snapping shrimp make flashing bubbles. *Nature* **413**, 477-478. doi:10.1038/35097152
- Longo, S. J., Goodearly, T. and Wainwright, P. C.** (2018). Extremely fast feeding strikes are powered by elastic recoil in a seahorse relative, the snipefish, *Macroramphosus scolopax*. *Proc. R. Soc. B* **285**, 20181078. doi:10.1098/rspb.2018.1078
- Longo, S. J., Cox, S. M., Azizi, E., Ilton, M., Olberding, J. P., St. Pierre, R. and Patek, S. N.** (2019). Beyond power amplification: latch-mediated spring actuation is an emerging framework for the study of diverse elastic systems. *J. Exp. Biol.* **222**, jeb197889. doi:10.1242/jeb.197889
- Muñoz, M. M.** (2019). The evolutionary dynamics of mechanically complex systems. *Integr. Comp. Biol.* **59**, 705-715. doi:10.1093/icb/icz077
- Muñoz, M. M., Anderson, P. S. L. and Patek, S. N.** (2017). Mechanical sensitivity and the dynamics of evolutionary rate shifts in biomechanical systems. *Proc. R. Soc. B* **284**, 20162325-. doi:10.1098/rspb.2016.2325
- Muñoz, M. M., Hu, Y., Anderson, P. S. L. and Patek, S. N.** (2018). Strong mechanical relationships bias the tempo and mode of morphological evolution. *Elife* **7**, e37621. doi:10.7554/eLife.37621
- Noh, M., Kim, S.-W., An, S., Koh, J.-S. and Cho, K.-J.** (2012). Flea-inspired catapult mechanism for miniature jumping robots. *IEEE Trans. Robot.* **28**, 1007-1018. doi:10.1109/TRO.2012.2198510
- Patek, S. N.** (2019). The power of mantis shrimp strikes: interdisciplinary impacts of an extreme cascade of energy release. *Integr. Comp. Biol.* **59**, 1573-1585. doi:10.1093/icb/icz127
- Patek, S. N. and Longo, S. J.** (2018). Evolutionary biomechanics: the pathway to power in snapping shrimp. *Curr. Biol.* **28**, R115-R117. doi:10.1016/j.cub.2017.12.033
- Patek, S. N., Korff, W. L. and Caldwell, R. L.** (2004). Deadly strike mechanism of a mantis shrimp. *Nature* **428**, 819-820. doi:10.1038/428819a
- Patek, S. N., Nowroozi, B. N., Baio, J. E., Caldwell, R. L. and Summers, A. P.** (2007). Linkage mechanics and power amplification of the mantis shrimp's strike. *J. Exp. Biol.* **210**, 3677-3688. doi:10.1242/jeb.006486
- Patek, S. N., Dudek, D. M. and Rosario, M. V.** (2011). From bouncy legs to poisoned arrows: elastic movements in invertebrates. *J. Exp. Biol.* **214**, 1973-1980. doi:10.1242/jeb.038596
- Patek, S. N., Rosario, M. V. and Taylor, J. R. A.** (2013). Comparative spring mechanics in mantis shrimp. *J. Exp. Biol.* **215**, 1317-1329. doi:10.1242/jeb.078998
- Patek, S. N., St. Pierre, R., Longo, S. J., Schelling, B. and Cox, S.** (2023). Geometric latches enable tuning of ultrafast, spring-propelled movements. *Dryad, Dataset* **215**, 1317-1329. doi:10.5061/dryad.sqv9s4n6k
- Reynaga, C. M., Eaton, C. E., Strong, G. A. and Azizi, E.** (2019). Compliant substrates disrupt elastic energy storage in jumping tree frogs. *Integr. Comp. Biol.* **59**, 1535-1545. doi:10.1093/icb/icz069
- Ribak, G.** (2020). Insect-inspired jumping robots: challenges and solutions to jump stability. *Curr. Opin. Insect Sci.* **42**, 32-38. doi:10.1016/j.cois.2020.09.001
- Ritzmann, R.** (1973). Snapping behavior of the shrimp *Alpheus californiensis*. *Science* **181**, 459-460. doi:10.1126/science.181.4098.459
- Ritzmann, R.** (1974). Mechanisms for the snapping behavior of two alpheid shrimp, *Alpheus californiensis* and *Alpheus heterochaelis*. *J. Comp. Physiol.* **95**, 217-236. doi:10.1007/BF00625445

- Roberts, T. J.** (2019). Some challenges of playing with power: does complex energy flow constrain neuromuscular performance? *Integr. Comp. Biol.* **59**, 1619–1628. doi:10.1093/icb/icz108
- Rosario, M. V. and Patek, S. N.** (2015). Multi-level analysis of elastic morphology: the mantis shrimp's spring. *J. Morphol.* **276**, 1123–1135. doi:10.1002/jmor.20398
- Rosario, M. V., Sutton, G. P., Patek, S. N. and Sawicki, G. S.** (2016). Muscle–spring dynamics in time-limited, elastic movements. *Proc. R. Soc. B* **283**, 20161561. doi:10.1098/rspb.2016.1561
- Sakes, A., Van Der Wiel, M., Henselmans, P. W. J., Van Leeuwen, J. L., Dodou, D. and Breedveld, P.** (2016). Shooting mechanisms in nature: a systematic review. *PLoS One* **11**, e0158277. doi:10.1371/journal.pone.0158277
- Schein, H.** (1977). The role of snapping in *Alpheus heterochaelis* Say, 1818, the big-clawed snapping shrimp. *Crustaceana* **33**, 182–188. doi:10.1163/156854077X00089
- Schindelin, J., Arganda-Carreras, I., Frise, E., Kaynig, V., Longair, M., Pietzsch, T., Preibisch, S., Rueden, C., Saalfeld, S., Schmid, B. et al.** (2012). Fiji: an open-source platform for biological-image analysis. *Nat. Methods* **9**, 676–682. doi:10.1038/nmeth.2019
- Schmitz, B. and Herberholz, J.** (1998). Snapping behaviour in intraspecific agonistic encounters in the snapping shrimp (*Alpheus heterochaelis*). *J. Biosci.* **23**, 623–632. doi:10.1007/BF02709175
- Silliman, B. R., Layman, C. A. and Altieri, A. H.** (2003). Symbiosis between an alpheid shrimp and a xanthoid crab in salt marshes of mid-Atlantic states, USA. *J. Crustac. Biol.* **23**, 876–879. doi:10.1651/C-2410
- St. Pierre, R. and Bergbreiter, S.** (2019). Toward autonomy in sub-gram terrestrial robots. *Annu. Rev. Control Robot. Auton. Syst.* **2**, 231–252. doi:10.1146/annurev-control-053018-023814
- Steinhardt, E., Hyun, N. P., Koh, J., Freeburn, G., Rosen, M. H., Temel, F. Z., Patek, S. N. and Wood, R. J.** (2021). A physical model of mantis shrimp for exploring the dynamics of ultra-fast systems. *Proc. Natl. Acad. Sci. USA* **118**, e2026833118. doi:10.1073/pnas.2026833118
- Sutton, G. P., St Pierre, R., Kuo, C.-Y., Summers, A. P., Bergbreiter, S., Cox, S. and Patek, S. N.** (2022). Dual spring force couples yield multifunctionality and ultrafast, precision rotation in tiny biomechanical systems. *J. Exp. Biol.* **225**, jeb244077. doi:10.1242/jeb.244077
- Tang, X. and Staack, D.** (2019). Bioinspired mechanical device generates plasma in water via cavitation. *Sci. Adv.* **5**, eaau7765. doi:10.1126/sciadv.aau7765
- Vermeij, G. J.** (1987). *Evolution and Escalation: An Ecological History of Life*. Princeton: Princeton University Press.
- Versluis, M., Schmitz, B., Von Der Heydt, A. and Lohse, D.** (2000). How snapping shrimp snap: through cavitating bubbles. *Science* **289**, 2114–2117. doi:10.1126/science.289.5487.2114
- Wainwright, P. C., Mehta, R. S. and Higham, T. E.** (2008). Stereotypy, flexibility and coordination: key concepts in behavioral functional morphology. *J. Exp. Biol.* **211**, 3523–3528. doi:10.1242/jeb.007187
- Winn, H. E. and Hazlett, B. A.** (1962). Sound production and associated behavior of Bermuda crustaceans (*Panulirus*, *Gonodactylus*, *Alpheus*, and *Synalpheus*). *Crustaceana* **4**, 25–38. doi:10.1163/156854062X00030
- Zack, T. I., Claverie, T. and Patek, S. N.** (2009). Elastic energy storage in the mantis shrimp's fast predatory strike. *J. Exp. Biol.* **212**, 4002–4009. doi:10.1242/jeb.034801
- Zhang, C., Zou, W., Ma, L. and Wang, Z.** (2020). Biologically inspired jumping robots: a comprehensive review. *Robot. Auton. Syst.* **124**, 103362. doi:10.1016/j.robot.2019.103362

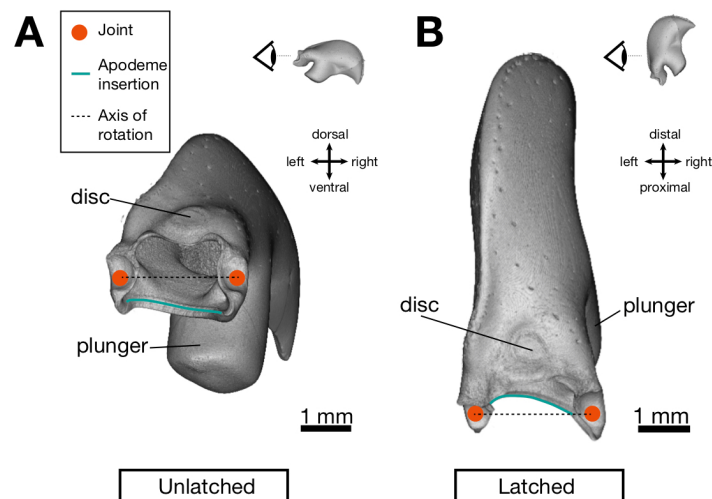


Fig. S1. Subtle features of dactyl morphology in *Alpheus heterochaelis* promote latching. **A.** When the dactyl is closed against the propodus, the joint (pivot) is above the apodeme insertion (turquoise line) to which the closer and trigger muscles attach. Posterior (proximal) view of the dactyl joint. **B.** To latch, the dactyl is opened and rotates into this position. The notched morphology of the dactyl causes the apodeme insertion (turquoise line) to pass above the axis of rotation (dashed line) formed by the dactyl joint. In this orientation, activation of the closer muscle will not generate a net closing torque on the dactyl. Visualization guides have been included in the upper right where terminology is with respect to a dactyl being observed by a viewer positioned as in A, and the adhesive disc and plunger have also been labeled to assist with orientation. Images are reconstructions from micro-CT scans of dactyl molts; apodemes were digitally removed for clarity.

Table S1. Morphological information for specimens included in this study.

Specimen ID	A5	A11	A13	A15	D001	D002	D003	JD4	JD2	pair1female
Total Mass (g)	0.9227	1.2858	0.2975	0.3488	0.6283	0.6674	0.6413	1.0460	0.92	0.6407
Claw Mass (g)	0.1274	0.2915	0.0391	0.0535	0.1359	0.1132	0.0813	0.1933	0.1411	0.1549
Total Length (mm)	32.75	34.70	23.85	24.32	28.50	31.41	30.64	34.17	33.12	25.53
Propodus length (mm)	12.89	16.62	9.24	9.86	13.10	12.74	11.32	15.43	14.04	13.05
Dactyl length (mm)	5.78	6.69	3.79	3.96	5.56	5.10	4.76	6.40	5.54	5.25
Sex	Didn't record	Male	Male	Male	Male	Female	Female	Male	Male	Female

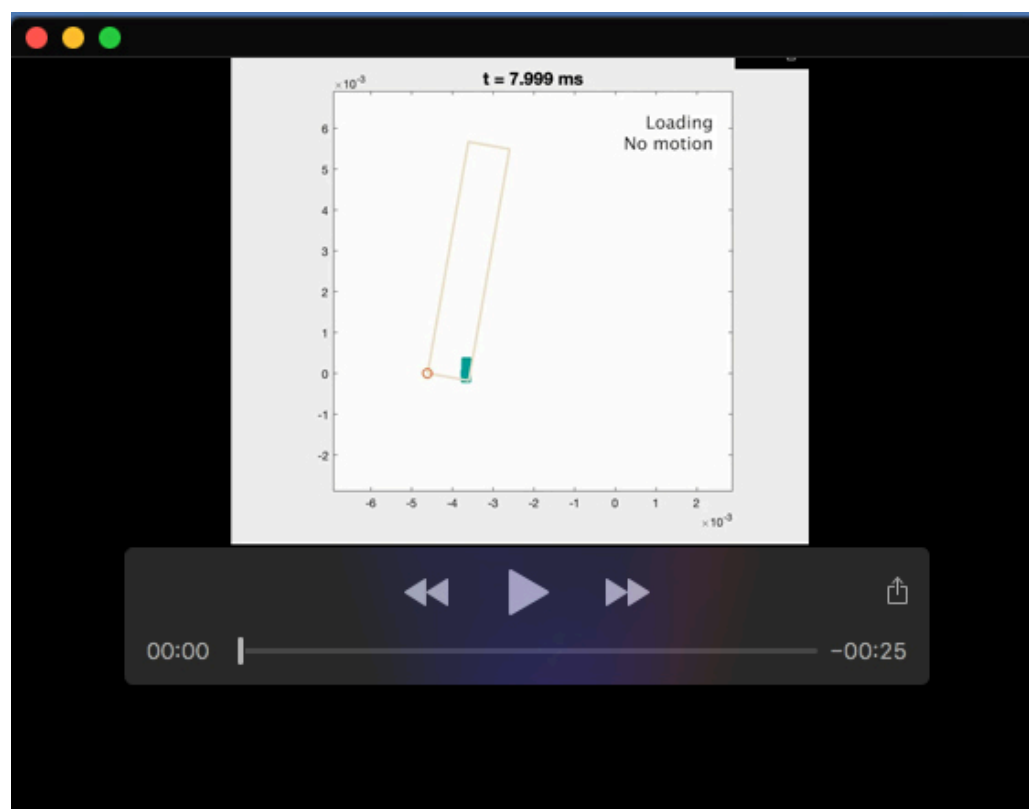
Note that 'JD2' and 'pair1female' are the identifications for specimens filmed only for analysis of propodus deformation. Total mass included the mass of the entire shrimp (including claw). Claw mass included both the dactyl and propodus. All masses are wet masses. Lengths were either measured directly on the specimen or using calibrated photos. JD2 mass is reported to two decimal points due to a recording oversight.



Movie 1. Example video demonstrating exoskeleton deformation during the loading phase before a strike. To emphasize propodus shape change, the video is played back approximately 4.25x slower than in real life. This loading phase is typical in duration (442.5 ms). Original filming rate: 50,400 fps; effective rate after subsampling: 128 fps; playback speed: 30 fps.



Movie 2. Example of a loading video followed by the corresponding strike video sequence. In each video, the shrimp can be seen in lateral view (top) and ventral view (using a mirror; below). The ventral view was used to determine dactyl motion, while the lateral image was used to check that the claw was oriented properly and not touching the tank bottom. This loading sequence took 391 ms and the strike took 0.81 ms. Note that the loading and strike sequences were originally filmed at 50,400 fps and then saved at different framerates to accommodate their different timescales. Loading sequence effective rate after subsampling: 504 fps; playback speed: 30 fps. Strike sequence: 50,400 fps no subsampling; playback speed: 30 fps.



Movie 3. Example loading and striking from the reduced-order model. During the simulation, the spring is loaded with energy, seen through the elongation of the animated spring. When the energy loading is complete, the unlatching process begins by rotating the spring opposite to the simulated dactyl motion (rectangular block). It should be noted that the time step changes from 1 ms to 1 μ s after torque reversal.